Severe haze episodes in Beijing may be influenced by emissions in far western China

Benjamin Foreback[1,2,3], Petri Clusius[2], Metin Baykara[2,4], Alexander Mahura[2], Lukas Pichelstorfer[2,5], Carlton Xavier[2,6,7], Putian Zhou[2,8], Tom Kokkonen[2,8], Veli-Matti Kerminen[2], Yongchun Liu[1], Men Xia[1], Xin Chen[1], Chenjie Hua[1], Zongcheng Wang[1], Roman Nuterman[9], Alexander Baklanov[9,10], Giancarlo Ciarelli[2,8], Victoria A. Sinclair[2], Zhi-Song Liu[11], Taiwo Ashu[3,11], Valery Ashu[3,11], Markku Kulmala[1,2,8], Pauli Paasonen[2], and Michael Boy[2,3,11]

[1]Aerosol and Haze Laboratory, Beijing Advanced Innovation Center for Soft Matter Science and Engineering, Beijing University of Chemical Technology, Beijing, China
[2]Institute for Atmospheric and Earth System Research / Physics, Faculty of Science, University of Helsinki, Finland
[3]Atmospheric Modelling Centre – Lahti, Lahti University Campus, Lahti, Finland.
[4]Climate and Marine Sciences Department, Eurasia Institute of Earth Sciences, Istanbul Technical University, Istanbul, Turkey
[5]pi-numerics, Neumarkt am W., Austria
[6]Department of Physics, Lund University, Lund Sweden
[7]Swedish Meteorological and Hydrological Institute (SMHI), Research Department, Unit of Meteorology/Environment and Climate, Norrköping, Sweden
[8]Nanjing-Helsinki Institute in Atmospheric and Earth System Sciences, Nanjing University, Nanjing, China
[9]Niels Bohr Institute, University of Copenhagen, Copenhagen, Denmark
[10]Department of Atmospheric and Oceanic Sciences, Fudan University, Shanghai, China
[11]School of Engineering Science, Lappeenranta-Lahti University of Technology (LUT), Lappeenranta, Finland

Corresponding author: Benjamin Foreback
Email: benjamin.foreback@helsinki.fi
ORCID: 0000-0002-5061-7098

Acknowledgements

The authors wish to acknowledge the Institute of Atmospheric and Earth System Research (INAR) for the opportunity to work on and develop this project, as well as the Atmosphere and Climate Competence Center (ACCC) flagship organization for its support in atmospheric science research in Finland, which made this project possible.

The authors would also like to acknowledge CSC – IT Center for Science, Finland, for computational resources, including high-performance computing on Puhti and Mahti HPC, as well as computational advice and support.

The background maps were made with Natural Earth's free vector and raster map data, available at naturalearthdata.com.

Abstract

We applied the FLEXPART (FLEXible PARTicle dispersion model) and SOSAA (the model to Simulate the concentration of Organic vapors, Sulfuric Acid, and Aerosols) modelling system to simulate a severe pollution episode in Beijing in November 2018. SOSAA conducts model calculations using a Lagrangian approach, moving with the transported air masses. The model includes detailed chemical and aerosol mechanisms, incorporating aerosol size distribution in addition to simple mass concentrations. This is particularly valuable from a health perspective because particles in the Aitken mode size range significantly impact health. In this study, SOSAA was run along 7-day backward trajectories to investigate the origins and processes of a severe haze episode in Beijing during November 2018. Our findings indicate that approximately 75% of the particles in Beijing originated from outside the city, resulting from regional rather than local emission sources. The highest pollutant concentrations during the peak of the haze episode were observed when trajectories passed through the high-emission region of southern Hebei province. Some of the particle mass during the haze was traced back to Xinjiang, a region with substantial industry and coal use. After evaluating the results, we created several reduced-emission scenarios and conducted sensitivity tests, which we applied to this haze episode. We discovered that comprehensive emission control across multiple emission sectors was more effective than addressing only one individual sector. Furthermore, we found that large-scale emission control at a regional or national level would be significantly more effective than merely restricting emissions within the city limits of Beijing.

1. Introduction

Due to China's rapid economic growth over the past several decades, there has been a significant focus on researching and understanding air quality in Chinese cities (Zeng et al., 2019; Wang and Hao, 2012; Fang et al., 2009). In addition to long-term averages, there has been a focus on studying severe haze episodes, which are especially prevalent during autumn and wintertime in the North China Plain (NCP), including the megacity of Beijing (Wu et al., 2021; Zhang et al., 2020a; Xiao et al., 2020; Zheng et al., 2016; Zheng et al., 2015a; Zheng et al, 2015b). Although on average, air pollutant concentrations can be between 10 and 100 times higher in Chinese cities than in European or North American cities, during extreme air pollution episodes, some pollutant concentrations can be over 1000 times higher (Kulmala, 2015). These episodes have serious short- and long-term consequences on human health, resulting in hospitalizations and premature deaths every year (WHO, 2024; Luo et al., 2021; Gao et al., 2015a; Ji et al., 2012; Jiang et al., 2015). Additionally, haze episodes can cause substantial economic losses costing millions of dollars, including, for example, medical costs and loss of working time (OECD, 2016; Gao et al., 2015a; Xie et al., 2019).

Haze episodes also impact regional meteorology through aerosol radiative feedback effects, and these effects can be spread over several thousand square kilometers in eastern China (Liu et al., 2018b; Gao et al., 2015b). Consequently, repeated and persistent large-scale episodes throughout the autumn and winter can have larger-scale climate effects (Baklanov et al., 2016). Conversely, several studies (e.g., Morawska et al., 2021; Cai et al., 2017; Westervelt et al., 2016; Zhang et al., 2018) have shown through modelling and historical analysis that climate change is influencing these pollution episodes, notably by increasingly setting up meteorological conditions that are favorable for pollution episodes to occur. These effects, therefore, create a feedback mechanism in which climate change sets up conditions for pollution episodes, and aerosol effects of widespread pollution episodes influence climate. Thus, studying and understanding

these widespread haze episodes is important from both a health and climate perspective. This includes understanding the origins of the episodes, such as the emission sources and precursors. It's also important to understand the lifecycles of haze episodes, including the chemical and physical processes that occur leading up to and during the episodes, and their eventual termination mechanisms.

Previous studies, including Wu et al. (2021), Chen et al. (2019), Sun et al. (2017), Huang et al. (2017), and Wang et al. (2017), have shown that during haze episodes, as much as half of the observed air pollution in Beijing is transported from the nearby region as opposed to originating from local sources. Wu et al. (2021) found that during the most severe pollution episodes, nonlocal emission sources contribute to 75% of the $PM_{2.5}$ concentrations. For this reason, Tong et al. (2019) suggest that emissions should be controlled at a regional rather than local level. A recent study by Ding et al. (2024) estimated that inter-provincial transport of pollutants was responsible for close to 40% of aerosol pollution-related deaths in 2017. Another recent study by Zhang et al. (2024b), which used satellite imagery to analyze the transport of atmospheric pollutants in China, described Beijing as a "haze sink" in terms of pollutants being transported into the Beijing area from other regions. This study particularly cited the geography and topography for trapping pollutants in the Beijing area.

In addition to short-range regional transport, several studies, such as Daellenbach et al. (2024), Lu et al. (2023), Yang et al. (2017), Wang et al. (2015), and Ni et al. (2018) have used observations and models to show that long-range transport can carry particulate matter and other pollutants over great distances in China. Yang et al. (2017) used trajectory modelling to show that particulate matter during a severe haze episode in Beijing could be transported from as far as Xinjiang and surrounding regions and countries.

Although several existing regional chemical transport models (CTMs), e.g. the Community Multiscale Air Quality Modeling System (CMAQ) and Weather Research and Forecasting coupled with chemistry (WRF-Chem), are utilized for air quality research and forecasting, these models include simplified aerosol dynamics. The most significant parameters in CTMs include PM_{10} (mass concentration of particles under 10 micrometers in diameter) and $PM_{2.5}$ (mass concentration of particles under 2.5 micrometers in diameter), along with trace gases, e.g., nitric oxides, carbon monoxide, ozone, and sulfur dioxide (Zhang et al., 2016; Thunis et al., 2016). For general reporting of day-to-day air quality to the public, measurements of PM and basic trace gases are typically adequate metrics (Snyder et al., 2013). However, these general air quality parameters have limitations when it comes to a holistic understanding of air quality; for example, there is not always international consistency in how these datasets are measured and reported (van den Elshout et al., 2008), and these parameters do not always give a full picture of the formation and processes behind poor air quality conditions (Kumar et al., 2015). Moreover, submicron particles—especially those in the Aitken mode size range (30-100 nm)—have significant impact on health because they can pass through the lungs and enter the bloodstream (Li et al., 2016; Han et al., 2016; Kwon et al., 2020). Therefore, size distribution is a valuable metric of air quality's impact on health in addition to PM mass concentration. This highlights the importance of understanding the chemical and physical processes that lead to the formation and lifecycle of haze and hazardous air quality.

For this study, we ran the model to Simulate the concentration of Organic vapors, Sulfuric Acid, and Aerosols (SOSAA) along hourly backward trajectories, generated with the FLEXible PARTicle dispersion model (FLEXPART), arriving in Beijing during and after a severe haze episode that occurred from November 11-15, 2018. By applying SOSAA to this episode, we can gain further knowledge and understanding of the emission sources, formation, lifecycle, atmospheric chemistry, and physical processes during the episode.

SOSAA's novelty is that it targets a specific site of interest and includes highly detailed chemical and aerosol processes which can be applied to air quality studies in megacities. This study examines atmospheric processes such as the source area of the airmass prior to the episode, emissions before and during the episode, and chemical reactions during the episode's lifetime. SOSAA also provides the particle number size distribution (PNSD) and chemical composition along the trajectories and at the arrival point throughout the study period.

After evaluating the model with station measurements in Beijing, we ran several hypothetical modified emissions scenarios and several sensitivity tests to investigate the model's sensitivity to changes in emissions. The main goal of these sensitivity tests is to gain insight on local versus regional sources and how changes to the system could influence the overall haze situation. The scenarios can also show how emission control regulations and air quality control measures could improve air quality and provide crucial information to policymakers and stakeholders.

The main scientific objectives of this study are as follows:

- Demonstrate and evaluate the FLEXPART-SOSAA modelling system during a late autumn haze episode in Beijing.
- Understand how the haze observed in Beijing formed and where the primary and secondary aerosol mass contributing to the haze originated. This includes quantifying the proportions of particle number and mass originating in Beijing, the Beijing-Tianjin-Hebei (BTH) region, and farther away, during the investigated haze episode.
- Determine how hypothetical reduced emission scenarios might impact this haze episode.
- Assess how different meteorological inputs and primary emissions datasets would influence the modelled outcomes.

2. Methods

In this study, we took a Lagrangian modelling approach, combined with air quality observations conducted at a measurement station in Beijing. We used backward atmospheric trajectories to trace airmass sources and emissions of primary particles and secondary organic aerosol (SOA) precursor gases, which resulted in the haze observed at the station. We ran SOSAA along the trajectories to simulate the processes leading up to the haze that arrived at the station. The final time point of each along-trajectory model run was used to create a modelled view of the station, and the results were compared to measurements from the station.

Figure 1 shows an overview of China with a hypothesized example of a trajectory that could transport atmospheric pollutants from high-emission areas into Beijing. The inset in this figure is a map of Beijing, pointing out the location of the measurement location.

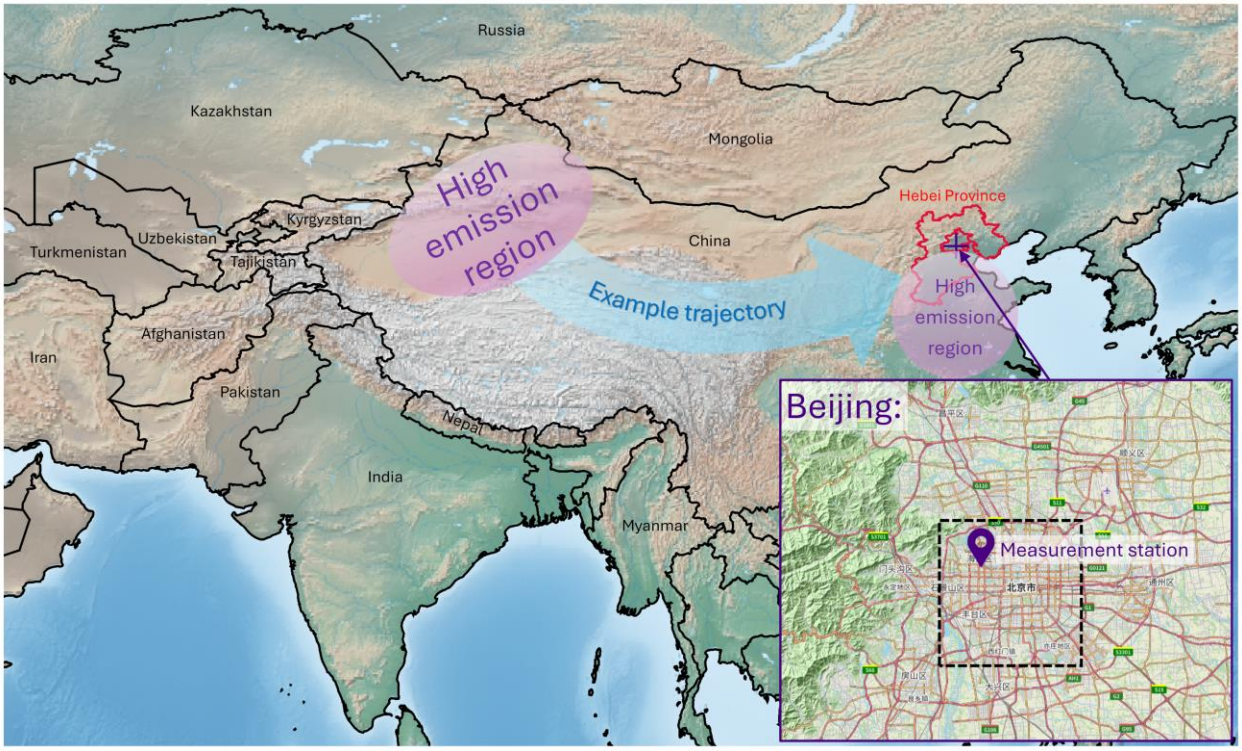

Fig. 1 Map of China and surrounding countries showing Hebei province in red, with the city of Beijing marked with a cross. This map shows an example of hypothesized long-range transport of pollutants to Beijing during the case study period. The inset shows a map of Beijing with the location of Beijing University of Chemical Technology's Aerosol and Haze Laboratory (BUCT-AHL) marked. The dashed line indicates the informal boundary between the city of Beijing and the surrounding region, which approximately follows the 5th Ring Road. Map data for Beijing is from OpenStreetMap. © OpenStreetMap contributors. Available under the Open Database License from https://www.openstreetmap.org

2.1. Case study period

Our case study focused on 13 days from 9 through 21 November 2018. This period includes the 11-15 November haze episode, two days day before, and several days after. On the 9th of November, the remnants of the previous haze episode were still evident. The 15th-18th of November was a period with cleaner air compared to the haze episode, which we hereafter refer to as the non-haze period. After the 18th of November, the beginning stage of the next haze episode was in process.

It is important to note that this study is based on a short case study, which includes a severe haze episode with very high concentrations of particles and gas pollutants. This study focuses on implementing the SOSAA modelling framework in a megacity environment, examining its sensitivity and showcasing the framework's usefulness and flexibility, while also providing a case study for a detailed investigation of pollution sources that lead to haze. Results of longer-term averages may be different from those of this study. This study does not aim to propose specific policy changes; instead, it may serve as a starting point for long-term studies, as it suggests potential areas for improvements in the model, input datasets, and environmental impact.

2.2. Measurement data

2.2.1. BUCT-AHL site

As part of the effort to study and understand haze and air quality in China, the University of Helsinki and Beijing University of Chemical Technology (BUCT) joined forces and combined expertise to build a long-term air quality measurement station in Beijing (Liu et al., 2020b; Peltonen 2017). The goal of the station, known as the BUCT Aerosol and Haze Laboratory (BUCT-AHL), is to collect continuous and comprehensive atmospheric meteorological, trace gas, and aerosol measurements. Continuous observations at BUCT-AHL began in February 2018 (Liu et al., 2020b). The station is based on the concept of the Station for Measuring Ecosystem-Atmosphere Relations (SMEAR) in Hyytiälä, Southern Finland (Liu et al., 2020b; Hari and Kulmala, 2005) and is part of the effort to build a global SMEAR network (Kulmala, 2018), with the aim to understand atmospheric chemical cocktail in megacities (Liu et al., 2020b; Kulmala, 2015).

This site is located near the Third Ring Road approximately 9 km west-northwest of the center of Beijing. The station's coordinates are 39° 56' 30" N 116° 17' 50" E, marked on the inset of Figure 1. The measurements site is on the rooftop of a five-story building, 18 meters above ground level, and it consists of a comprehensive set of aerosol, trace gas, and meteorological instruments. This study used the data from these instruments to evaluate SOSAA.

For the analysis, we utilized the SOSAA output level at 52.5 meters above ground. Although this is somewhat higher than the BUCT-AHL station, we used this level to make it more representative of the area and ensure that surface interactions did not influence the results in the urban environment (Liu et al., 2018a).

Size distribution data at BUCT-AHL, which we used in this project for model evaluation, are from the Particle Size Magnifier (PSM) for particles with diameters between 1.3 and 1.85 nm, the Neutral cluster & Air Ion Specter (NAIS) for particles between 1.85 and 10 nm in diameter, and the Differential Mobility Particle Sizer (DMPS) for particles greater than 10 nm in diameter, up to 840 nm. There is some overlap in sizes between the NAIS and the DMPS (The NAIS measures up to 40 nm, and the DMPS measures as small as 6 nm), so we chose 10 nm as the cutoff between the two for the most seamless results. When comparing PM mass between SOSAA and the measurements, we calculated mass from the DMPS's full range. We did not include mass from the PSM or NAIS in this calculation because the mass from particles < 6 nm is negligible compared to the total mass. When comparing the modelled mass to the measurements, we used $PM_{0.84}$, which corresponds to the DMPS measurement range. Details of the instruments and the measurement site at BUCT-AHL can be found in Liu et al. (2020b).

2.2.2. Other data sources

To analyze the meteorology in the synoptic context, we downloaded surface and 500 hPa weather charts from the Digital Typhoon database, created by the Japan Meteorological Agency (Digital Typhoon, 2024). Specifically, we used the Asia Pacific Surface Analysis, produced every 12 hours (00 and 12 UTC daily). We have annotated these figures and have included them in the supplementary material.

In addition to the meteorology data measured at BUCT-AHL, we also obtained historical weather data from Beijing Capital International Airport (PEK), which we downloaded from Weather Underground (Weather Underground, 2024).

For further analysis of the haze episode, we used $PM_{2.5}$ data from a China-wide network of real-time air quality sensors, which are managed by the Ministry of Environmental Protection (MEP) and published hourly by the China Environmental Monitoring Centre (CEMC; Song et al. 2017; Tao et al. 2016).

2.3. Modelling Framework

Figure 2 provides a detailed illustration of the FLEXPART-SOSAA modelling framework, including inputs and outputs, described in the following subsections.

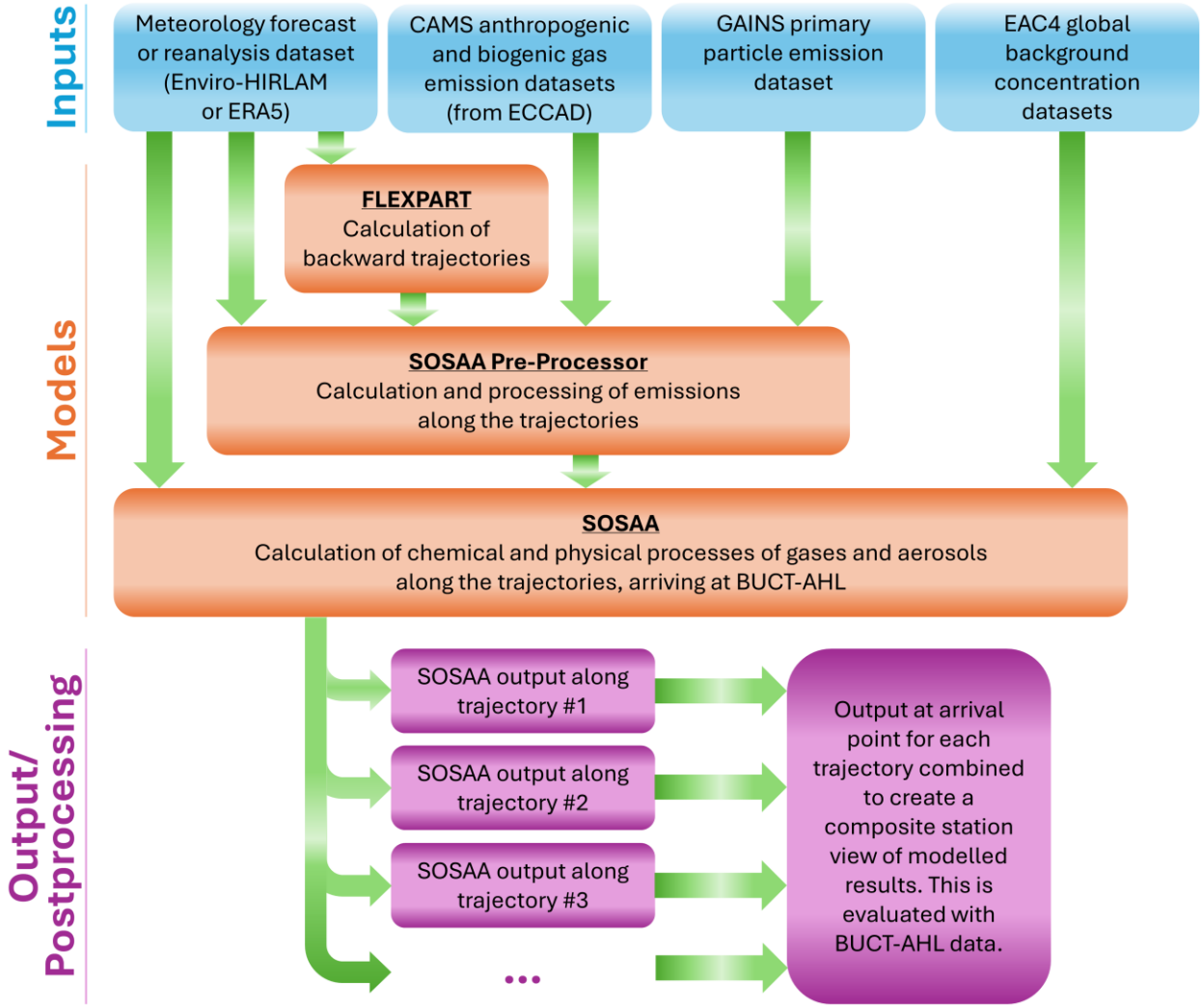

Fig. 2 The workflow of the FLEXPART-SOSAA modelling system used in this study

Simulations for this project were performed on high-performance computers (HPC) maintained by CSC – IT Center for Science, Finland. Details about the computing environments used for this project can be found in Appendix A of Foreback et al. (2024) and on the CSC website: https://docs.csc.fi/computing

2.3.1. Meteorological Input

The modelling process started with a Numerical Weather Prediction (NWP) dataset. Two different NWP input datasets have been used in this project to compare SOSAA sensitivity to different meteorological inputs. Doing so offers us more confidence in our results in cases where separate results when using different meteorological inputs closely agree. For this study, we used the inputs described below, which are further described in Foreback et al. (2024), a project on which this study was built.

Enviro-HIRLAM

Enviro-HIRLAM (the Environment – High-Resolution Limited Area Model; Baklanov et al., 2017) is an online integrated limited-area NWP and CTM modelling system, which can be run on multi-scales, and it is a part of the Pan-Eurasian Experiment – Modelling-Platform (PEEX-MP; Mahura et al., 2024). It uses HIRLAM NWP as a baseline for meteorology. The "Enviro" refers to the integrated CTM part of the model, i.e., chemistry and aerosol processes and atmospheric transport, dispersion and deposition of chemical species, and in particular, aerosols. Feedback mechanisms of aerosols, including direct aerosol effects on solar radiation and indirect aerosol effects on solar radiation due to their impacts on cloud formation, are seamlessly integrated into Enviro-HIRLAM's weather prediction (Baklanov et al., 2017). In other words, it considers chemical and aerosol effects in numerical weather forecasting. This can be significant in a region which frequently experiences high aerosol concentrations, such as the greater BTH region (Sun et al., 2015, 2016). In this highly industrial region, high concentrations of aerosols can significantly influence direct and indirect aerosol effects, affecting local meteorology (Zhang et al., 2019; Korsholm et al., 2010). Baklanov et al. (2017) demonstrated that Enviro-HIRLAM meteorological forecasts performed better when aerosol effects were included. Therefore, we hypothesized that using Enviro-HIRLAM meteorology input for this study could yield more realistic results than models that do not account for aerosol effects, especially considering the exceptionally high aerosol concentrations during the series of pollution episodes in November 2018.

For this project, we set up Enviro-HIRLAM runs for November 2018, and the runs were conducted four times using the following cases:

- Combined Direct and Indirect Aerosol Effects (CAE), which included both direct and indirect aerosol effects.
- Direct Aerosol Effect (DAE), which included only the direct effects of aerosols on solar radiation and the related feedbacks on meteorology.
- Indirect Aerosol Effect (IAE), which included only the indirect effects of aerosols on solar radiation via clouds and cloud radiative feedbacks.
- No Aerosol Effects (NAE), which executed meteorological forecasts without including any effects of aerosols on the meteorology. Note: In Foreback et al. (2024), this was called the control/reference case, but hereafter, we will refer to this case as NAE to avoid confusion with the base case of this study.

Throughout this study, we used the CAE meteorology for the base case in FLEXPART-SOSAA. The sensitivity studies and scenarios are modified from this base case. We also ran FLEXPART-SOSAA sensitivity tests using the outputs from the Enviro-HIRLAM DAE, IAE, and NAE runs as meteorological input to FLEXPART and SOSAA (described in section 2.5).

For the Enviro-HIRLAM runs, we set up nested/downscaled domains as follows:

- 0.25-degree (approx. 25 km) horizontal resolution outermost domain covering most of Eurasia, extending from west-central Europe to eastern China and the Yellow Sea of the Pacific Ocean. This domain extends more westward from Beijing than eastward because all trajectories during this case study originated from the west, consistent with the prevailing winds.
- 0.15-degree (approx. 15 km) domain extending over China, Mongolia, and the Korean Peninsula.
- 0.05-degree (approx. 5 km) domain extending over eastern Mongolia, eastern and northern China, through the Yellow Sea.
- 0.025-degree (approx. 2.5 km) domain, the innermost domain with highest horizontal resolution, covering Beijing-Tianjin-Hebei and the surrounding urban region.

Section 2.2.1 of Foreback et al. (2024) describes the details of the Enviro-HIRLAM runs used in this study. Figure 2 of that paper shows a map of the downscaled/nested domains used in the runs. Baklanov et al. (2017) describes the technical details of the Enviro-HIRLAM model, including downscaling methods.

ERA5

In addition to Enviro-HIRLAM meteorology for FLEXPART-SOSAA, we used the European Centre for Medium-Range Weather Forecasts (ECMWF) Reanalysis version 5 (ERA5) meteorological datasets (Hersbach et al., 2020) with hourly temporal resolution. These datasets originated from the IFS (Integrated Forecast System) model at spectral truncation T639 (which corresponds to 0.28° resolution at the equator). For this study, we used the Flex_Extract software (Tipka et al., 2020) to obtain global ERA5 datasets at $0.25° \times 0.25°$ horizontal resolution, which is the highest extraction resolution available.

2.3.2 FLEXPART Back-Trajectories

The back-trajectories used in this study were generated with FLEXPART, a Lagrangian model for simulating air parcel transport and dispersion. It can be run in either forward mode (i.e., tracing the dispersion after a point release) or backward mode (i.e., tracing back the source of an air parcel). The out-of-the-box FLEXPART 10.4 package (the version we used in this study), downloaded from the FLEXPART website, can take in meteorological forecasts or reanalysis datasets from ECMWF, such as the ERA5 datasets (mentioned above), or from the U.S. National Center for Environmental Prediction (NCEP), such as the Global Forecast System (GFS) forecast or analysis datasets (Pisso et al., 2019). Additionally, we implemented an adaptation to FLEXPART so that it can also use Enviro-HIRLAM modelled output as its meteorological input. This adaptation is published in Foreback et al. (2024).

For this study, we generated back-trajectories with arrivals in Beijing every hour, and hourly time steps were used within each FLEXPART trajectory simulation. For the 13-day study period mentioned above, this resulted in a total of 321 trajectories. Meteorology used from both the Enviro-HIRLAM output and ERA5 datasets was taken at the same hourly time steps as FLEXPART, and we ran the trajectories seven

days back in time from the station of interest. FLEXPART was set up with a horizontal grid size of 0.1 degrees for all runs, and the grid interpolation between the meteorology datasets and trajectory model is handled within FLEXPART. Each trajectory simulated 40,000 hypothetical particles arriving at BUCT-AHL.

The output of each FLEXPART trajectory simulation contains a gridded value called source-receptor relationship (SRR). The term SRR can be used interchangeably with potential emission sensitivity. Hereafter, we will use the term SRR. In layman's terms, the SRR is the footprint of the backward trajectory that is used to determine how much time the trajectory spent over a specific area. The unit of SRR is seconds (Pisso et al., 2019), and this value can be multiplied by the emission rate for the particular grid cell/area, to determine the total emissions into the trajectory at the given time. Details of the SRR are described in Pisso et al. (2019) and Seibert and Frank (2004). The average trajectory (i.e., the single line drawn on a map) is the average of the SRR values at each time step along the trajectory. For calculation of emissions along each trajectory, SOSAA uses the SRR values (described in the next section), but for simplicity in visualization, the average trajectories are shown on the maps in Section 4.

Foreback et al. (2024) provide more details about the FLEXPART runs used for this case study. Technical details about FLEXPART can be found on the FLEXPART website, http://flexpart.eu, and in Pisso et al. (2019), Stohl et al. (1998), Stohl and Thompson (1999), and Stohl et al. (2005).

2.3.3. Emission datasets and pre-processing

After creating the back-trajectories, we used the Copernicus Atmosphere Monitoring Service (CAMS; Granier et al., 2019) inventories for gas emissions and the Greenhouse Gas–Air Pollution Interactions and Synergies (GAINS; Amann et al., 2011; Paasonen et al., 2016) inventory for particle number emission to gather emission rates along the trajectories.

The CAMS datasets were obtained through the Emissions of Atmospheric Compounds and Compilation of Ancillary Data (ECCAD) portal. This was done using the SOSAA pre-processor (SPP) script. The script used the SRR in the trajectories, found the corresponding grid point in the emission datasets, along with a weighted average of nearby grid boxes, at each time step, and multiplied the emission with the SRR value from FLEXPART. The resulting values were saved to a file that was provided to SOSAA.

For this study, we downloaded the following CAMS datasets from the ECCAD portal on 5 April 2024:

- Anthropogenic (ANT): Version 5.3, monthly (Soulie et al., 2024).
- Biogenic (BIO): Version 3.1, monthly (Sindelarova et al., 2022, 2014).
- Oceanic (OCE): Version 3.1, daily (Ziska et al., 2013; Nightingale et al., 2000; Lana et al., 2011).
- Ship (SHIP): Version 3.2, daily (Jalkanen et al., 2016, 2012; Johansson et al., 2012, 2017).
- Soil (SOIL): Version 2.4, monthly (Simpson et al., 2023).
- Temporal (TEMPO): Version 2.1, daily (Guevara et al., 2020, 2021).

To determine continental anthropogenic primary particle emissions, we used datasets produced with the GAINS model, which include annual gridded particle number emission and size distributions. The SPP script temporalized the annual emissions from GAINS into hourly emission rates along each trajectory based on the SRR and the CAMS temporal datasets mentioned above. Each emission sector in GAINS was matched with the equivalent sector in the CAMS temporal dataset.

Dust emission was calculated in SPP using the methodology described by Leung et al. (2023) and Kok et al. (2014). The dust calculation used the Regridded Harmonized World Soil Database v1.2 (Wieder et al., 2014).

2.3.4. SOSAA Model

SOSAA is a vertical, one-dimensional atmospheric chemistry and aerosol dynamics model developed at the University of Helsinki, and it has been proven effective as a stationary column model (Chen et al., 2021; Zhou et al., 2014; Boy et al., 2011). In this project, SOSAA was adapted to run along back-trajectories generated with FLEXPART. By piecing together trajectories arriving every hour, we could take the SOSAA output at arrival time and create a stationary view of air quality in Beijing.

For this study, we ran SOSAA with 30-minute modelled time steps along each trajectory, while some modules within the model were run with higher temporal resolution. For example, emission input and chemistry were done with one-minute time steps, aerosol simulation with 30-second time steps, and mixing with 10-second time steps. Because the trajectories crossed multiple time zones, our simulations were performed using UTC. In the results of this study, analysis along trajectories uses UTC, and analysis at the arrival in Beijing uses Beijing local time (UTC+8 year-round).

In this study, we set up SOSAA with 45 vertical levels from the surface up to 2500 meters, fully encompassing the boundary layer through the entire study period. Height levels in SOSAA are defined as fixed heights above ground level in meters. Each level in SOSAA incorporates chemistry and aerosol dynamics through the same methodology as the Atmospherically Relevant Chemistry and Aerosol box model (ARCA box), introduced in Clusius et al. (2022).

SOSAA's main driver of chemistry is the Master Chemical Mechanism (MCM) version 3.3.1 (Jenkin et al., 1997, 2003, 2015, 2015; Saunders et al., 2003; Bloss et al., 2005). In addition to the full MCM chemistry, SOSAA incorporates the Peroxy Radical Autoxidation Mechanism (PRAM) developed by Roldin et al. (2019) to represent autoxidation from isoprene and monoterpene. Currently under development in SOSAA is the inorganic and organic particle-phase chemistry module.

Furthermore, because concentrations of aromatics are considerably higher in China compared to other parts of the world (Zhang et al., 2015), considering the chemical transformation of aromatics in the atmosphere is important to model air quality in China accurately. Pichelstorfer et al. (2024) introduced a new framework called the Automated Alkoxy/Peroxy Radical Autoxidation Mechanism Framework (autoAPRAM-fw). The new framework was used to generate autoxidation chemistry schemes for the most significant aromatics, which substantially improved the aerosol dynamics in the ADCHEM model. The aromatic autoxidation chemistry generated by the autoAPRAM-fw has since been integrated into SOSAA and was incorporated into this case study.

Cluster formation was simulated using the Atmospheric Cluster Dynamics Code (ACDC), using an ion-mediated H_2SO_4–DMA and H_2SO_4–NH_3 system, based on the DLPNO-CCSD(T) method, as described in Olenius et al. (2013) and Besel et al. (2020). We used an ion production rate of 3 cm^{-3}. The organic nucleation module in SOSAA is described by Zhou et al. (2014). We used the method from Nannoolal et

al. (2008) to determine vapor pressures for condensable vapors. In this model setup, we used 60 logarithmically distributed particle size bins ranging from 1 to 2000 nm in diameter.

Ozone is an important oxidant in atmospheric chemistry. While a significant amount of tropospheric ozone is produced through chemical reactions near the surface, some tropospheric ozone is transported downwards from the stratosphere (Williams et al, 2019; Hess et al., 2015), which is a process not included in SOSAA. To account for this, SOSAA reads the ozone background concentrations at each time step from the CAMS reanalysis – EAC4 datasets (Inness et al., 2019), which we downloaded from the Copernicus data store. Due to the long-lived nature of CO (1-2 months), we have done the same for CO, but only at the first time step.

Previous analysis using SOSAA found that the model tends to overestimate SO_2 concentrations. One possible reason is that SOSAA is a dry model which does not include droplet activation, cloud processes, or heterogeneous chemistry of SO_2. Cloud processes are a sink of SO_2 (Roldin et al., 2011), and heterogeneous oxidation of SO_2 is an important mechanism for sulfate formation from SO_2 during haze episodes in Asia (Su et al., 2020). However, many current models are missing these processes (Ma et al., 2023). Moreover, in environments with high aerosol loadings, such as a haze episode in Beijing, multiphase sulfate formation can occur even in cloud-free conditions (Liu et al., 2021; Liu et al., 2020a). These processes are not included in SOSAA, and thus, we are likely underestimating the SO_2 sinks in the model and consequently overestimating SO_2 concentrations when the trajectories arrive in Beijing. Furthermore, there has been a rapid decline in SO_2 emissions in China over the past few decades, and the emissions inventories used for models may have uncertainties and may not be up to date with the decline in emission rates (Cao et al., 2021; Sun et al., 2018; Ni et al, 2018; He et al, 2012). To account for the overestimation of emissions and the unaccounted-for mixed-phase and wet processes, we multiply the SO_2 emissions by 0.25.

2.4. Statistical evaluation of model performance

To evaluate SOSAA's performance in Beijing, we compared the results of SOSAA at the hourly arrivals of trajectories with the BUCT-AHL measurements using the mean fractional bias (MFB) and mean fractional error (MFE). The criteria for the model adequately representing the data are that $|MFB| < 60\%$ and $MFE < 75\%$ (US EPA, 2007). We then placed the results on a "soccer goal plot" with the criteria highlighted on the plot. This plot also has a goal area of $|MFB| < 30\%$ and $MFE < 50\%$; however, the criteria area is considered acceptable. We did this analysis for each of the pollutants individually: PM, NO_2, NO_x, CO, and SO_2. For each of these pollutants, we tested thrice: once for all times, once for the haze period, and once for the non-haze times.

To evaluate the scenarios and sensitivity tests, we used the Mann-Whitney test, which shows whether two datasets are statistically different. We chose this test because, unlike a simple t-test, the Mann-Whitney test does not assume a normal distribution, and it is not based on the mean, which could be influenced by some extreme values. In this case, we are investigating a haze episode which may contain some extremely high pollutant concentration values, and there is significant variation in the data; for example, for some pollutants, there may be an order of magnitude difference in concentration between the haze and non-haze periods.

For each test case (i.e., modelled scenario or sensitivity test) and each pollutant variable within each test case (the same pollutants used for the soccer goal plots), we passed the concentration values of the base case and the concentration values of the test case into the Mann-Whitney test and obtained the Z-score and the p-value. Since the Mann-Whitney test is a test of the sameness of two populations and we are interested in showing that the test case is statistically different, we will hereafter look at 1–p instead of p itself. To confidently show that the test case is statistically different from the base case, we aim for $1–p > 0.95$. Furthermore, if we want to say that the test case resulted in an improvement in air quality, we want $Z < 0$, indicating that the test case has lower concentrations than the base case (if $Z > 0$, the test case increased the pollutant concentration and thus did not improve air quality). Combining statistical analysis with sensitivity testing serves as a good way to identify areas where the model algorithms can be improved and where future work can be focused (US EPA, 2007).

2.5. Scenario analysis and sensitivity tests

After we ran SOSAA for the base case, we created three alternate emission scenarios to test the model's sensitivity to emissions changes and to simulate the resulting air quality during this haze period in these scenarios. These three scenarios are intended to be based on realistic changes that could be made, based on current research.

We also created several additional sensitivity tests, which, although not necessarily intended to be realistic future scenarios, can be used to identify potential improvements for the model and to test the sensitivity that different inputs have on the resulting air quality simulations. Table 1 summarizes each of the test cases (scenarios + sensitivity tests) used in this study, and they are described further in the subsections below.

Category	Case name	Description
Base case	Base case	Simulation with Enviro-HIRLAM CAE meteorological input for the FLEXPART trajectories. Chemistry includes the full MCM chemistry, autoxidation and SOA formation from isoprene and monoterpene is calculated using PRAM, and autoxidation of anthropogenic aromatics using code generated from autoAPRAM-fw.
Reduced emission scenarios	Scenario 1: Electric cars	Simulation of a scenario with 25% of cars in the BTH region switched to electric, based on Jiang et al. (2023).
	Scenario 2: Regional emission control	Reduced traffic, residential, industrial, and electricity generation emissions in the BTH region. Based on Sun et al. (2021), Tong et al. (2019), Zhao et al. (2017), and Xue et al. (2016).
	Scenario 3: Emission control in Beijing only	Same as Scenario 2 above, but only in the city of Beijing rather than the whole BTH region. This is used to demonstrate the importance of implementing regional emission controls when addressing air quality.
Local sources versus transport	Zero emission in Beijing	All emissions within the city of Beijing removed to quantify how much of the observed pollution is transported from outside the city versus sourced within the city.

No agricultural waste burning	AWB was set to zero throughout the entire model domain.	This tests the effect of eliminating AWB, especially for concentrations of larger particles.
Different meteorological inputs	Enviro-HIRLAM DAE	Same as base case but using Enviro-HIRLAM DAE meteorological input for FLEXPART trajectories and meteorology in SOSAA.
	Enviro-HIRLAM IAE	Same as base case but using Enviro-HIRLAM IAE meteorological input for FLEXPART trajectories and meteorology in SOSAA.
	Enviro-HIRLAM NAE	Same as base case but using Enviro-HIRLAM NAE meteorological input for FLEXPART trajectories and meteorology in SOSAA.
	ERA5	Same as base case but using IFS-ERA5 meteorological input for FLEXPART trajectories and meteorology in SOSAA. This serves as a reference to compare the results using Enviro-HIRLAM and the FLEXPART version developed in Foreback et al. (2024) to the results using the out-of-the-box version of FLEXPART.
Anthropogenic and biogenic VOC emissions that may be unaccounted for	Double VOC emission	Tests the effect that some VOCs, which may be unaccounted for in the model, would have on the results.

Table 1 Description of the scenarios and sensitivity tests used in this study

2.5.1. Modified emissions scenarios

The first two alternative emission scenarios focused on the BTH region, emphasizing regional air quality control measures. The reason to focus on regional emission control and air quality mitigation strategies rather than on only the city of Beijing is due to transport from outside the city. To evaluate this in our model, we created a third scenario that simulates emission control only in the city of Beijing, so that regional vs. local emission reduction can be compared.

For modelling purposes, we have simplified the BTH region as a box extending from 37.5 through 42 degrees north latitude and 114 through 118.5 degrees east longitude. This includes the cities of Beijing, Tianjin, Tangshan, Cangzhou, Baoding, and Shijiazhuang, along with the surrounding region, altogether with a population of 113 million residents (Wang et al., 2022). Inside this area, we modified the emissions inventories to represent the following scenarios, and outside of the region, we did not modify the emissions.

For simplicity in modelling, this study uses a sector-based approach. That is, emissions from whole sectors (e.g. traffic, industry, etc.) were reduced by a certain fraction. We did not modify emissions of individual compounds within each sector.

Scenario 1: Electric cars in the BTH region

This scenario is based on Jiang et al. (2023), and considers the introduction of battery electric cars, with no other emission control measures considered. In this scenario, we ran SOSAA with road transportation emissions (gases and primary particles) reduced by 25% in the BTH region to simulate the transition to zero-emissions battery electric cars.

Because electric cars need electricity to operate, this scenario is unrealistic without generating extra electricity to charge the electric cars. Jiang et al. (2023) explain that switching to electric cars would likely increase pollutant emissions from thermal power plants in the BTH region. Therefore, in our scenario run, we increased emissions in the electricity generation sector in the BTH region by 5% to compensate for the electricity demand that would be incurred by introducing electric cars.

Scenario 2: Comprehensive emission controls in the BTH region

This scenario includes the introduction of electric cars described in Scenario 1, and it also considers emission control measures in the transportation, industry, power generation, and residential sectors. This is intended to represent realistic air quality control measures which could be implemented in the greater BTH region. This scenario is based on Sun et al. (2021), Tong et al. (2019), Zhao et al. (2017), and Xue et al. (2016), and it includes changes in emissions for the following sectors:

- **Road transportation**: In addition to the introduction of electric cars, this scenario also considers emission controls mentioned in Sun et al. (2021), such as cleaner and more fuel-efficient gasoline vehicles and increased use of public transportation. Altogether, for this scenario, we reduced road transportation sector emissions in the BTH region by 40%.
- **Electricity generation/energy production:** This includes the higher demand for electricity due to the increase in electric cars. On the contrary, stricter emission controls on power plants, cleaner fuel, and demand reduction strategies can significantly lower emissions (Tong et al., 2019). Furthermore, this scenario considers an estimate of replacing 10% of electricity generation with solar power (Zhao et al., 2017), which has no direct emissions. Combining these considerations, we estimate a 35% reduction in emissions from electricity generation in this scenario.
- **Industry:** Additionally, this scenario will include strict emission control measures, along with the likelihood of some industries relocating outside of the BTH region (Tong et al., 2019), where we estimate a 50% reduction in industry emissions.
- **Residential heating and cooking:** Over 30% of $PM_{2.5}$ observed in Beijing is from residential heating and cooking, much of which is from coal burning (Zhang et al., 2024a; Xue et al., 2016; Zhang et al., 2017). There is currently an effort to reduce residential coal usage, and Xue et al. (2016) predict that up to 20% of residential heating and cooking will switch away from coal, most of which will become electric. In this scenario, we will assume a 20% reduction in residential heating and cooking emissions, and we will assume it switches to electric (as opposed to a different combustion fuel, which would introduce a new form of emissions).

Scenario 3: Comprehensive emission controls, but only in the city of Beijing

In this scenario, we used the same conditions as in Scenario 2, but only within Beijing. This scenario was created to test the importance of region-wide emission controls, as opposed to emission controls only within the city limits of Beijing. As mentioned by Tong et al. (2019), emission controls must be done in a wider area than just the city to mitigate air quality problems effectively. We defined the city as a box from

39.75 through 40.02 degrees north latitude and 116.2 through 116.54 degrees east longitude, approximately following Beijing's 5th Ring Road. This is marked as the dashed black line in the inset of Figure 1. The reason we chose the 5th Ring Road is because it has been used in the past as a boundary for emission restrictions (e.g., Wang et al., 2023; Liu et al., 2019; Sun et al., 2014).

2.5.2. Other sensitivity tests

Eliminating all anthropogenic emissions in Beijing

As a continuation of Scenario 3, the Beijing-only case, we tested the model with all anthropogenic emissions from all sectors set to zero in Beijing, using the same latitude/longitude box defined in Scenario 3. This sensitivity test aims to quantify the fraction of pollutant concentrations observed in Beijing from local sources within the city versus those transported from outside into the city.

Eliminating agricultural waste burning (AWB)

Recent efforts have been made to reduce the pollution from AWB, a common practice in China and other parts of the world during the post-harvest season (Cheng et al., 2022; Zhang et al., 2020b). This sensitivity test investigates the impact of AWB by setting all gas and primary particle emissions from AWB to zero throughout the entire model domain.

Different meteorological input data

In addition to the base case, which uses Enviro-HIRLAM CAE as the input, we ran the FLEXPART-SOSAA suite four times using the Enviro-HIRLAM DAE, IAE and NAE output and the ERA5 meteorology (described in section 2.3.1).

Increased VOCs

Although we included the autoxidation mechanisms for the most relevant biogenic VOCs and the most significant aromatics, we still lack the autoxidation mechanisms for many biogenic and anthropogenic VOCs in SOSAA. In particular, the autoxidation of several VOCs (e.g., alkanes and polyaromatics) is still not included in SOSAA, which could be significant in a region like China with high anthropogenic emissions. Therefore, we set up a sensitivity test with double VOC emissions to investigate the impact of increased VOCs in the model on particle formation and growth.

3. Observations during the study period

3.1. $PM_{2.5}$ measurements in Beijing during the haze episode

Throughout the autumn of 2018, Beijing and the NCP experienced a series of particularly severe haze episodes, reported by several international news outlets, including Reuters (Reuters, 2018). The 11th–15th November episode was one of the most severe, when some air quality observation stations in Beijing measured concentrations of particulate matter under 2.5 micrometers in diameter ($PM_{2.5}$) exceeding 200

μg/m^3. This was more than double the Chinese National Ambient Air Quality Standards (NAAQS) 24-hour average limit of 75 μg/m^3 and 13 times the World Health Organization's 24-hour air quality guideline value of 15 μg/m^3 (Ministry of Ecology and Environment, 2016; WHO, 2021).

$PM_{2.5}$ measurements during this haze episode averaged from 35 MEP stations in Beijing are shown in Figure 3. The episode followed a typical pattern described by Zheng et al. (2015b), Zheng et al. (2016) and Shen et al. (2020). It began with a slow buildup of pollutants over several days, and it ended with rapid cessation resulting from a synoptic weather feature involving a significant change in airmass. This is the most common type of pollution episode in Beijing in the autumn and winter (Zheng et al., 2016; Ji et al., 2012). Consistent with this pattern, the highest pollutant concentrations in Beijing during the episode were observed on the last two days of the episode, the 13th and 14th. These two days are considered severe winter haze days, defined by a daily mean $PM_{2.5}$ concentration of more than 150 μg/m^3 (Dang and Liao, 2019).

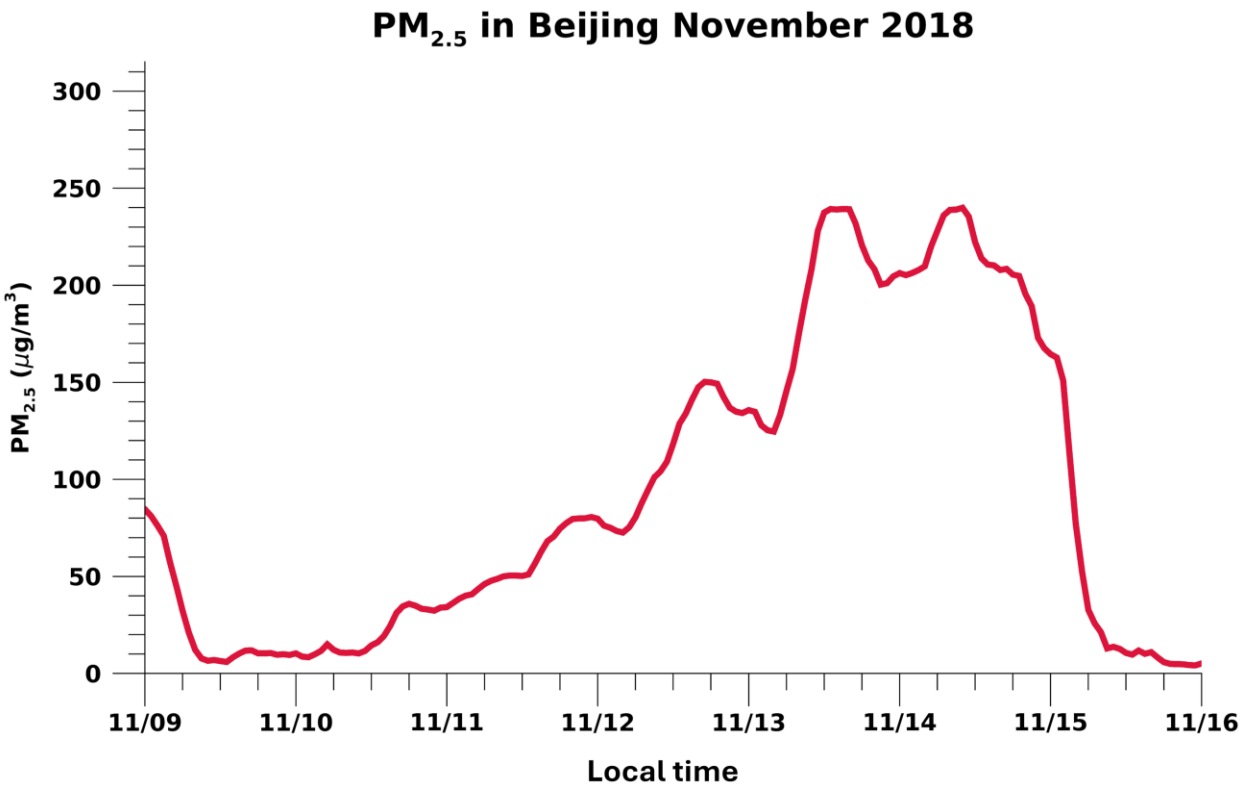

Fig. 3 Average of $PM_{2.5}$ concentrations from 35 monitoring stations throughout Beijing during the severe air pollution episode in November 2018 studied in this paper. Time is shown in Beijing local time.

3.2. Analysis of meteorological conditions before, during and after the haze episode

Haze is defined as the time when visibility is less than 10 km and relative humidity is less than 90% (Cai et al., 2022; Dang and Liao, 2019; Yang et al., 2016; Liu et al., 2013). This is seen in the BUCT-AHL meteorological measurements (Figure S1 in supplementary material) from November 11th through 15th,

although the conditions leading up to the haze, seen in this figure and in Figure 3 begin to take shape as early as the 10th of November.

Figure 4 shows satellite imagery of the haze episode's progression over northern China. These images make it clear that the hazy conditions were not localized to Beijing, as the widespread haze covered most of the North China Plain, nearly a thousand kilometers across.

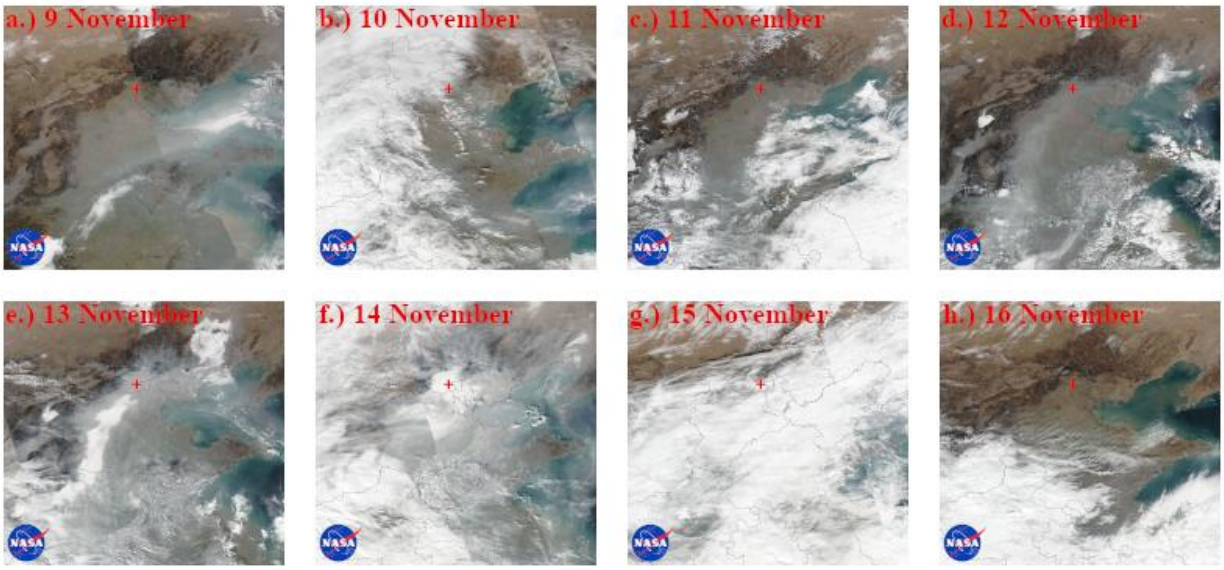

Fig. 4 Visible satellite imagery over northeastern China from the Visible Infrared Imaging Radiometer Suite (VIIRS) on the Suomi-NPP satellite: (a) 9 November as the previous pollution episode was subsiding; (b) 10 November, in the early stages of the episode. Beijing, noted by the red cross, was obscured by clouds; (c) 11 November as the episode was gradually building up; (d) 12 November as the episode continued to accumulate; (e) 13 November as the episode continued toward its peak; (f) 14 November, at the peak of the haze episode, when haze and clouds became indistinguishable; (g) 15 November when clouds obscured the region; (h) 16 November, after the pollution episode subsided and the air appeared clean. Each image was captured shortly after noon local time. The imagery shows a square of approximately 1000 by 1000 km.

The conditions for this haze episode began to occur on 9 November, shortly after the previous haze episode had subsided. In the satellite imagery shown in Figure 4(a), remnants of the previous haze episode were still visible when the satellite took the image shortly after noon, which is also seen in the $PM_{2.5}$ concentrations shown in Figure 3. According to meteorological observations at BUCT-AHL (Figure S1) and from weather reports at Beijing Capital International Airport (PEK), strong winds were from the north or northwest throughout the day, with gusts over 50 km/hr (14 m/s) reported at PEK late morning and early afternoon. The winds reduced in the evening, and by 23:30 local time, there were variable winds of only 4 km/hr. By 18 UTC (2:00 am local time), the archived surface weather charts (Figure S2) showed a high-pressure center, with a surface pressure of 1028 hPa, setting in over the Beijing region, which formed a blocking high-pressure system. This persistent high-pressure system remained in place throughout the haze episode.

On 10 November, some clouds were visible in the satellite image (Figure 4(b)). At this point, the high-pressure center had set in place over Beijing, with surface pressure reaching 1032 hPa, according to surface meteorological charts (Figure S3). This chart indicates widespread high pressure, along with light and variable winds throughout northern and eastern China. The uniform high pressure is a common characteristic of haze episodes in the autumn (Zheng et al., 2015b), and low wind speeds typically lead to accumulating pollutant concentrations over time without clean air being transported into the region and polluted air being transported away (Zheng et al., 2015a). By this time, the 500 hPa chart (Figure S4) showed the formation of a north-south oriented ridge over Beijing and the NCP, somewhat consistent with an omega block. This ridge remained in place for several days. Observations at PEK and BUCT-AHL showed light and variable wind throughout the day. By evening, the wind had shifted more toward a southerly direction. An additional high-pressure center was observed over Mongolia, a common characteristic of synoptic conditions which set up haze episodes in northern China (Zheng et al., 2015b; Yan et al., 2021).

The observed meteorological conditions remained almost identical from 11 through 13 November. Observations at BUCT-AHL showed significantly degraded visibility and reduced solar radiation during this time (Figure S1(c)). High pressure remained in place, and conditions were mostly stagnant. The surface high-pressure system continued to persist as a blocking pattern (Figure S5), and a ridge in the 500 hPa geopotential heights remained in approximately the same place throughout the haze episode period (Figure S6). This period was the buildup stage of the haze episode, which can be seen clearly in the $PM_{2.5}$ concentrations in Figure 3. The surface wind was variable but primarily from the southerly direction. These synoptic weather conditions, especially the persistent high pressure, are typical conditions during heavy, widespread haze episodes (Zheng et al., 2015a; Zheng et al., 2015b; Zheng et al., 2016). Besides the high-pressure center near Beijing, the pressure remained quite uniform across northern and eastern China throughout this several-day period, with surface pressure over 1020 hPa.

On 13 November, PEK airport station measured 100% relative humidity, and clouds in addition to the widespread haze became evident in the satellite imagery (Figure 4(e)). At 18:00 UTC (02:00 am local time), the blocking high-pressure system weakened slightly and finally moved eastward towards the coast, and a low-pressure system moved toward the north of Beijing (Figure S7).

By 14 November, the peak of the haze episode, the clouds and haze became almost indistinguishable in the satellite imagery (Figure 4(f)). In the surface chart for 12:00 UTC (20:00 local time; Figure S8), the low-pressure system north of Beijing moved eastward, which brought a small surface trough. Meanwhile, the high-pressure system that previously persisted over the region moved out to sea. The ridge in the 500 hPa chart (Figure S9) likewise moved to the east, towards the sea. Visibility at BUCT-AHL was less than 2 km (Figure S1(c)).

At 00:00 UTC (08:00 am local time) on 15 November, noticeable changes in weather conditions were observed in the Beijing region. According to the surface chart (Figure S10), the low-pressure system north of Beijing and the associated surface trough had moved eastward. The ridge in the 500 hPa weather chart (Figure S11) had already moved away from the Beijing region and out to sea. The pressure gradient and higher winds at 500 hPa can be seen in this chart. The changing weather system brought a shift in wind, along with a cleaner and drier airmass from the northwest. This new airmass was enough to almost completely clear out the haze episode within a few hours.

By 16 November, the new and clean airmass fully entered Beijing and the surrounding area. The surface chart (Figure S12) shows that the previous high-pressure system had moved far out to sea. The haze episode and weather system were gone, and clear, cloudless air was visible over Beijing in the satellite imagery (Figure 4(h)). $PM_{2.5}$ concentrations were less than 10 $\mu g/m^3$, indicating that the air pollution episode subsided. The 500 hPa chart (Figure S13) shows that most of China saw nearly perfectly zonal flow, with no significant weather systems in the region.

Within a few days, a new high-pressure system took shape over Mongolia, and a slack pressure gradient started to move in. This set up the conditions for the next haze episode to form, thus repeating the cycle of haze episodes.

4. Modelled results for the base case

4.1. Back-trajectories and airmass regions

Before investigating the modelled results at the station, we looked at the backward trajectories used in this study to gain insight into the context of the pollution source areas and the history of the airmasses that were observed arriving at the station. Understanding the history of the airmasses, especially the exposure to anthropogenic emission areas, is crucial for understanding aerosol processes and subsequent haze in Beijing (Hakala et al., 2022). The trajectories analyzed in this study are the same ones created and discussed in Foreback et al. (2024).

Previous studies, such as Wang et al. (2019), Huang et al. (2017), Hua et al. (2018), and Sun et al. (2015, 2016) have shown that southern Hebei province (i.e. the region to the south and southwest of Beijing) is an area of high pollution emissions. In contrast, the mountainous regions to the north and west of Beijing have fewer pollution sources due to lower population. The area in southern Hebei province is a heavy source of primary particles and gaseous atmospheric pollutants, which are precursors to the haze observed in Beijing. Therefore, airmasses which come from the south and southwest and pass through this region would likely have high concentrations of pollutant gases and particulate matter when they arrive at the station.

Looking farther west, beyond the region surrounding Beijing, studies such as Yang et al. (2019) and Xu et al. (2017) point out significant emission sources in western China, including the northern Xinjiang region. Although this region is mostly rural outside a few cities such as Ürümqi, there are heavy sources of coal combustion, as well as residential wood and coal burning in the cold seasons (Yang et al., 2019). This compounds the heavy emissions in the last few days along the trajectories before arriving in Beijing.

Backward trajectories before, during, and after the haze episode are plotted in Figure 5. The lines show the mean trajectories calculated by FLEXPART, plotted for arrivals every 12 hours (00 and 12 UTC). This figure clearly shows that the trajectories arriving during the haze episode (i.e., with the highest concentrations of pollutants) had previously been in this area of southern Hebei province, which is consistent with the previous research. We also see that all the trajectories arriving during the haze episode previously passed through western China, including the notably coal-heavy regions. Conversely, the

trajectories arriving after the episode originated farther northwest and passed through Mongolia (a lower-emission region) rather than western China.

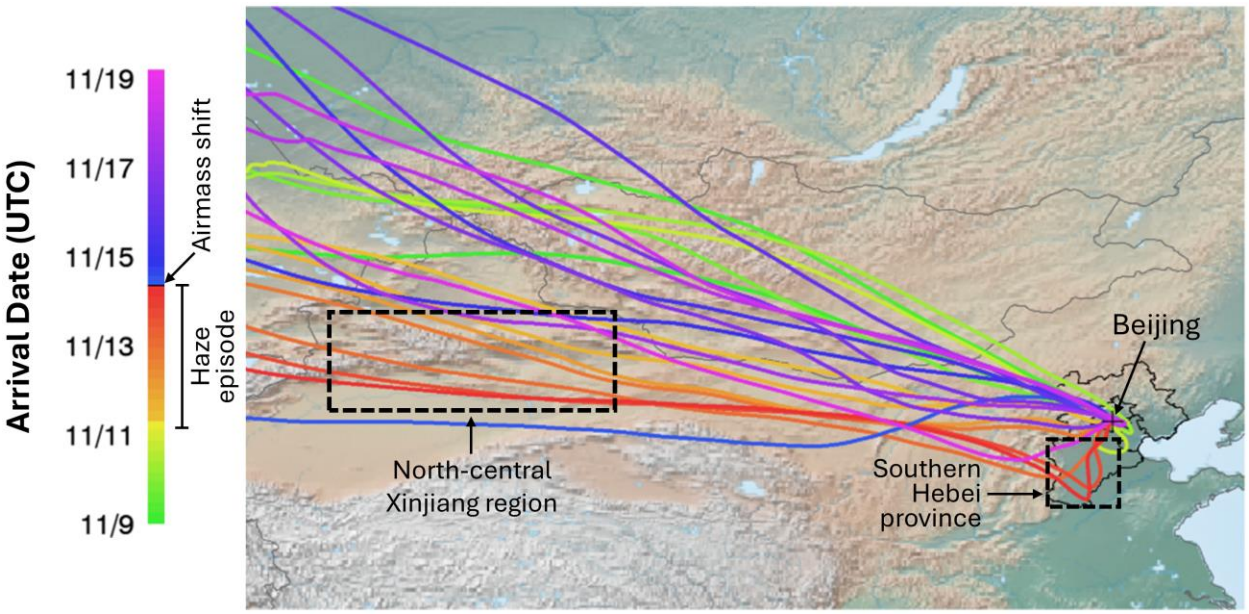

Fig. 5 Atmospheric backward trajectories arriving in Beijing from 9 through 19 November 2018, plotted at 12-hour intervals, each going back 7 days. The lines show the average trajectories calculated using FLEXPART with Enviro-HIRLAM CAE meteorological input. The investigated haze episode from 11-15 November is shown in brighter orange and red colors, which ended abruptly in the early morning of 15 November local time (late on 14 November in UTC) when an airmass shift brought clean air and a shift in wind speed and direction. Beijing Municipality, Tianjin Municipality, and Hebei Province (collectively BTH) are shown in the outlined area on the map. Southern Hebei province and north-central Xinjiang region, known as regions with heavy emission sources leading to pollution, are annotated with dashed boxes.

We also suspect that during the stagnant meteorological conditions of the haze episode, the airmasses observed at the station spent longer in the polluted area, which would result in more pollutant concentration buildup. We further analyzed this in Table 2, where we report the time that the average trajectories shown in Figure 5 spent inside southern Hebei and northern Xinjiang, which are the areas marked in the dashed boxes in Figure 5. Table 2 also reports the total SRR values inside the same areas.

Arrival time (Day, Month, time in UTC)	**Southern Hebei Region**		**Northern Xinjiang Region**	
	Time avg. traj. spent in region (h)	**Total SRR value (h)**	**Time avg. traj. spent in region (h)**	**Total SRR value (h)**
9 Nov. 00:00	0	0	0	75.90
9 Nov. 12:00	0	0	0	4.93
10 Nov. 00:00	0	0.01	0	36.07
10 Nov. 12:00	0	1.42	0	17.64
11 Nov. 00:00	8	11.32	0	14.85
11 Nov. 12:00	0	8.51	8	29.36

12 Nov. 00:00	0	0	27	42.81
12 Nov. 12:00	0	3.25	32	39.94
13 Nov. 00:00	0	20.61	37	32.29
13 Nov. 12:00	22	115.89	39	10.61
14 Nov. 00:00	33	73.11	36	5.38
14 Nov. 12:00	39	63.77	36	4.60
15 Nov. 00:00	0	5.00	0	7.12
15 Nov. 12:00	0	0	13	9.62
16 Nov. 00:00	0	0	0	0
16 Nov. 12:00	0	0	0	0
17 Nov. 00:00	0	0	0	3.30
17 Nov. 12:00	0	0.19	0	3.76
18 Nov. 00:00	0	0	44	12.25
18 Nov. 12:00	0	0	0	8.53
19 Nov. 00:00	0	0.04	0	6.61
19 Nov. 12:00	7	18.01	17	28.05

Table 2 Amount of time each average trajectory (the line which is calculated as the average trajectory) spent in the southern BTH and northern Xinjiang regions, along with each trajectory's total SRR values (first level only) inside the southern BTH and northern Xinjiang regions. This has been calculated using the Enviro-HIRLAM CAE as the meteorological input to FLEXPART. These are the same trajectories that are plotted in Figure 5. The haze episode is highlighted in gray.

The results shown in Table 2 confirm what we see visually in Figure 5, that the airmasses observed at the station during the haze episode, especially during the peak of the episode, spent time in the high-emission regions of southern Hebei and northern Xinjiang prior to arrival. We will investigate the potential origins of the haze in the next few sections.

4.2. Along-trajectory analysis of SOSAA

After investigating the trajectories and the source regions of airmasses arriving during and after the haze episode, we explored the particle number size distribution (PNSD) modelled by SOSAA along the trajectories. This along-trajectory analysis of PNSD is unique to SOSAA and is a novelty of this project, which in-situ measurements or other models do not offer. Figure 6 shows four example trajectories, where (a) and (b) arrived during the buildup of the haze episode, (c) arrived during the peak of the episode, and (d) arrived a day after the episode ended.

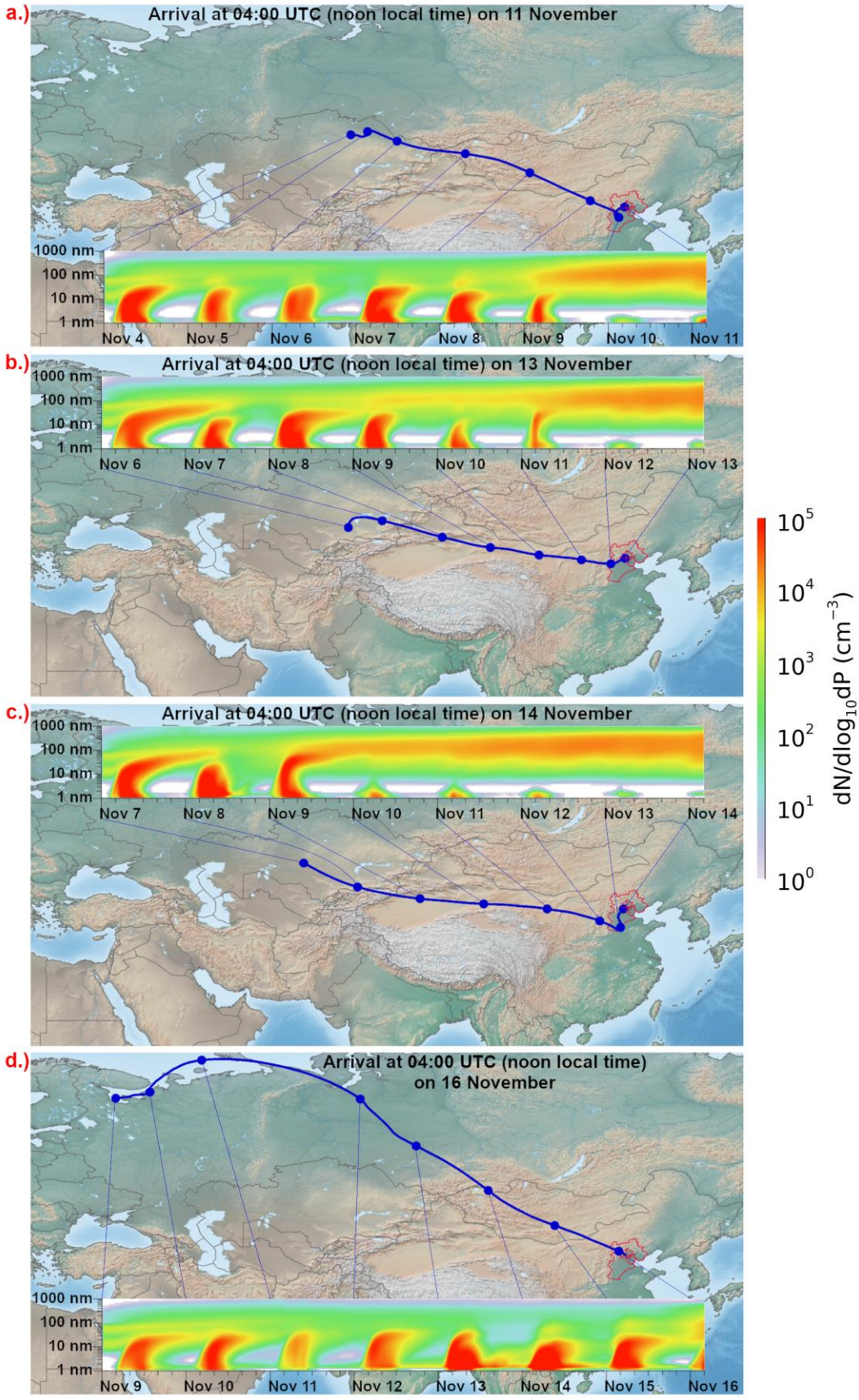
a.)
Arrival at 04:00 UTC (noon local time) on 11 November
1000 nm
100 nm
10 nm
1 nm
Nov 4
Nov 5
Nov 6
Nov 7
Nov 8
Nov 9
Nov 10
Nov 11
b.)
Arrival at 04:00 UTC (noon local time) on 13 November
1000 nm
100 nm
10 nm
1 nm
Nov 6
Nov 7
Nov 8
Nov 9
Nov 10
Nov 11
Nov 12
Nov 13
c.)
Arrival at 04:00 UTC (noon local time) on 14 November
1000 nm
100 nm
10 nm
1 nm
Nov 7
Nov 8
Nov 9
Nov 10
Nov 11
Nov 12
Nov 13
Nov 14
d.)
Arrival at 04:00 UTC (noon local time)
on 16 November
1000 nm
100 nm
10 nm
1 nm
Nov 9
Nov 10
Nov 11
Nov 12
Nov 13
Nov 14
Nov 15
Nov 16
10^5
10^4
10^3
10^2
10^1
10^0
$dN/dlog_{10}dP\ (cm^{-3})$

817

Fig. 6 Example of modelled particle number size distribution along four trajectories arriving in Beijing during the study period. Panels (a) and (b) show trajectories which arrived during the haze episode's buildup. Panel (c) shows a trajectory that arrived during the peak of the episode. Panel (d) shows a trajectory that arrived after the haze episode, after the passage of a weather system, which brought a clean airmass from a different direction.

We can see clearly in Figure 6(a) through (c) that the high concentrations of Aitken and accumulation mode particles (diameter > 30 nm) began not in Beijing but rather upwind several days earlier, becoming apparent as the trajectories entered the high-emission areas of northern and western China. In panels (b) and especially (c), we see that the high Aitken and accumulation mode concentrations began in the Xinjiang region of western China, as far as 2000 km west of Beijing.

Figure 6(d) shows a completely different airmass coming from a different region on 16 November after the haze episode had subsided. This trajectory did not pass through the same heavy-emission areas, such as the southern BTH region or northern Xinjiang. Instead, it entered directly into the Beijing region from the northwest, where there are fewer local emissions. Farther back, this trajectory arrived from Mongolia and Siberia, which are low-emission areas. Additionally, the higher wind speeds on 16 November resulted in the trajectory spending less time over local emissions in the immediate Beijing region. Therefore, this airmass brought much lower particles and gas pollutant concentrations than the trajectories arriving during the haze episode.

We notice that once the high Aitken and accumulation mode particle concentrations became apparent along the trajectories, new particle formation (NPF) was suppressed due to the high condensation sink (CS) values. After the episode, the trajectory shown in Figure 6(d), which had much lower Aitken and accumulation mode particle concentrations, NPF events occurred up until the day of arrival.

4.3. Arrival at BUCT-AHL and time series of all trajectory arrivals

Next, we pieced together the PNSD at arrival times for the entire 13-day period (312 hourly arrivals) to offer a simulated stationary picture of PNSD in Beijing. This is what an observer at a fixed point would see over time, and thus, we can compare this resulting PNSD to the measurements at BUCT-AHL. This is shown in Figure 7, with the SOSAA simulated PNSD at the arrival point over time in panel (a) and the observed PNSD from the DMPS, NAIS, and PSM instruments shown in panel (b).

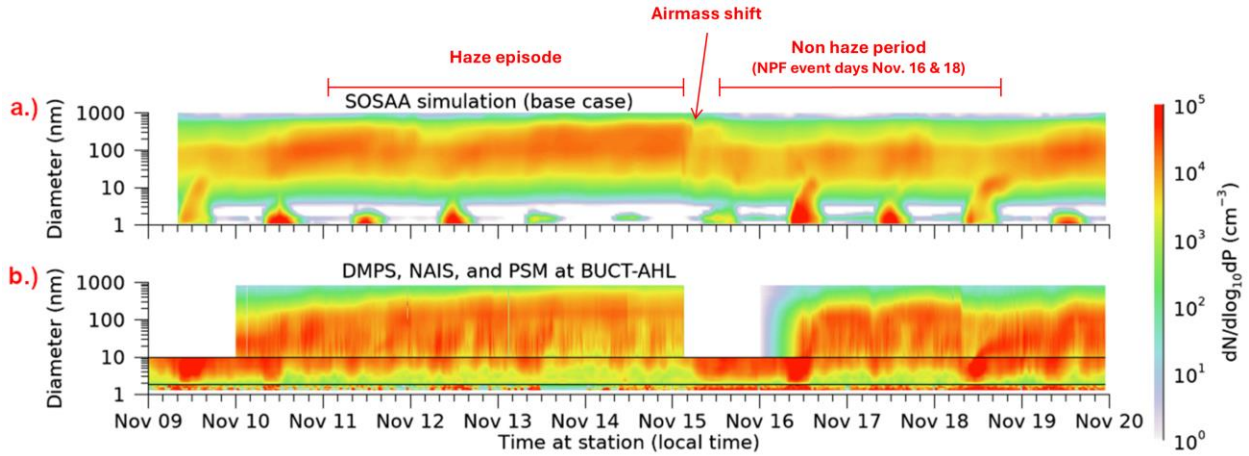

Fig. 7 Particle number size distribution in Beijing in November 2018. The modelled results from the SOSAA base case simulation are shown in panel (a). Panel (b) shows measurements at the BUCT-AHL station in Beijing as follows: PSM from 1.3 to 1.85 nm, NAIS from 1.85 to 10 nm, and DMPS from 10 to 840 nm.

The model captures the differences between the haze and non-haze periods quite well, and the change in airmass due to the synoptic weather shift is well-defined in the model. The model shows new particle formation in < 5 nm size range on most days, but the formed particles are scavenged by coagulation during the haze episode due to the high CS before their growth can be observed. Both the model and measurements show that NPF events resulting in growing particles occurred on 9, 16 and 18 November. However, the model does not show the NPF events as strongly as the measurements. Moreover, the model underestimates particle concentrations below about 40 nm in diameter throughout this case study. We investigated this further in Figure 8, which shows the differences between the model and measurements from Figure 7, along with histograms of the differences.

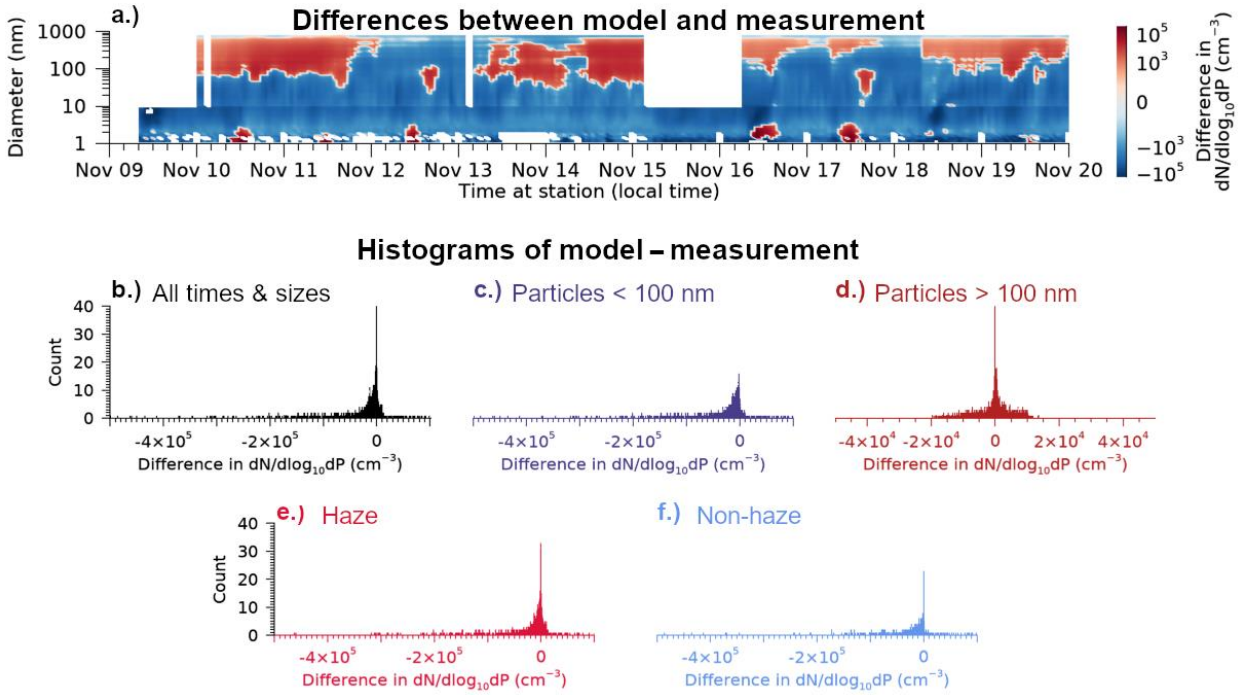

Fig. 8 (a) Differences between the modelled particle number size distribution and the measurements at BUCT-AHL. (b)-(f) show histograms of differences for different sizes and times. The histogram count indicates the number of times the PNSD differences in (a) were of the specified value, with bin sizes of 10 cm^{-3}

The histograms in Figure 8(b-d) show the model biases, which are split into ultrafine particles (<100 nm in diameter) and larger particles (>100 nm in diameter) and into haze and non-haze times. The model tends to underestimate ultrafine particle concentrations. At some points, the modelled concentration of ultrafine particles is nearly zero in the model, despite the observations showing the presence of such ultrafine particles. The model underestimates particle concentrations slightly more during the non-haze period. In particular, as shown in Figure 8(a), the model underestimates the particle formation events and subsequent growth on November 9, 16, and 18, likely contributing to the underestimation shown in Figure 8(f). On the other hand, the model mostly overestimates particles >100 nm in diameter on November 10th and 11th, in the early stages of the episode, and also on the 14th and 15th, at the peak of the episode.

A study by Wang et al. (2023a) using the Goddard Earth Observing System atmospheric chemistry (GEOS-Chem) model showed similar results for ultrafine particles, which were underestimated by the model. However, GEOS-Chem did not have the overestimation for >100 nm particles. Wang et al. (2023a) cited uncertainty in emissions as one of the likely causes for model bias, and the difference between the primary emission dataset used in GEOS-Chem versus SOSAA could explain the different result.

A possible explanation for the observed bias in SOSAA is that the GAINS primary particle emission dataset underestimates the emission of small particles while overestimating the emissions of larger particles. The underestimation of nucleation mode particle emissions by GAINS is expected (Paasonen et

al., 2016; Xausa et al., 2018), especially for traffic (Rönkkö et al., 2017). The overestimation of accumulation mode particles has not been observed previously (Xausa et al., 2018).

Another possible reason that SOSAA underestimates ultrafine particles, particularly during NPF events, is that SOSAA could be underestimating VOC concentrations, which are the precursors for particle formation and growth. We have created a sensitivity test that doubles VOCs, mentioned in Section 2.5.2, which we will evaluate in Section 5.5.

Next, examined not only one fixed height point but also the modelled vertical profile of particles at the station, shown in Figure 9. Simulating the vertical profile is unique to the model because such measurements are not available from station measurements during this period.

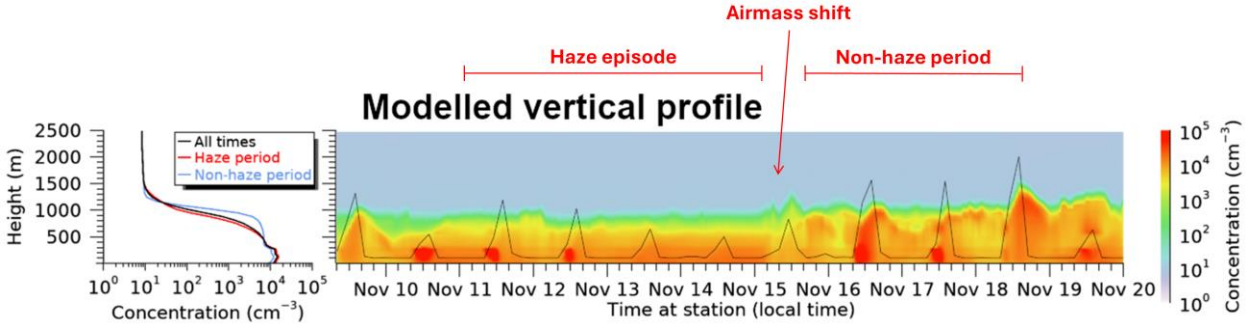

Fig. 9 Vertical profile of particle concentration modelled by SOSAA. The black line over the particle concentrations indicates the boundary layer height, which is taken from the Enviro-HIRLAM meteorological dataset.

We see in Figure 9 that during the haze episode, especially from 13 -15 November, the haze is uniform and well-mixed within the boundary layer. The boundary layer height is quite low at night, exacerbating the particle concentrations and haze. After the weather system passes, the boundary layer is higher, more turbulent, and less uniform. There is more diurnal variation in boundary layer height during the non-haze time. Although values of number concentration are not necessarily significantly less during the non-haze period, the mass, composition, and age of the particles are quite different between the two time periods, which we investigate in the next section.

4.4. Particle mass, composition, and age

SOSAA can track the age of primary and SOA mass. This is a novelty of SOSAA and something that is difficult to do with measurements without a specific tracer that can be tracked in the atmosphere. Figure 10 shows $PM_{0.84}$ mass from SOSAA compared to $PM_{0.84}$ mass calculated from the DMPS, as well as the composition and age of primary and SOA particles, which are colored by the day of emission/formation. This figure also shows the mass fraction of inorganics and dust, but the model does not keep track of the age of these compounds.

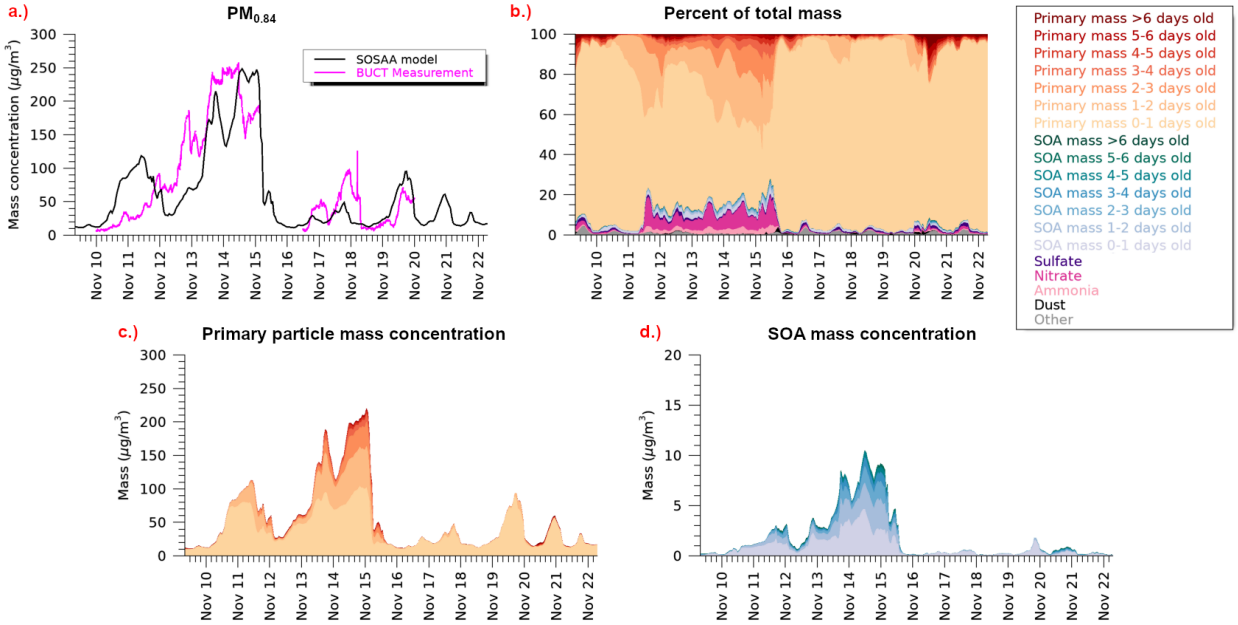

Fig. 10 (a) $PM_{0.84}$ mass concentration modelled by SOSAA compared to total mass calculated from the DMPS, which has a maximum measured particle size of 0.84 μm. (b) fraction of total mass of primary particles colored by age (based on the day of emission), SOA colored by age (based on the day of formation), and other aerosols, including inorganics. (c) the total particle mass of primary particles colored by age, and (d) SOA mass colored by age

In Figure 10(a), we can see that the overestimation of larger particles noted in Figure 8 significantly impacted the mass concentrations on November 10th and 11th, resulting in the model overestimating the mass concentration of $PM_{0.84}$. This overestimation of the mass is also evident immediately before the cessation of the episode late on November 14th and early on the 15th.

Figure 10(b) shows that during the haze period, nearly 80% of the simulated particle mass was from primary emissions. During the episode, about 5% of the particle mass was from SOA, and up to 10% was from inorganics, with these fractions increasing as the episode progressed. During the non-haze period, the contribution of SOA and inorganic mass was much smaller, with the model showing as much as 95% of the $PM_{0.84}$ mass from primary sources.

Two measurement studies were ongoing during this haze episode and the period before and after. Cai et al. (2022) studied organic aerosols and composition at the BUCT-AHL site, and Shen et al. (2020) used mass spectrometry to analyze chemical composition at a location east of Beijing. SOSAA and the measurement studies showed qualitative agreement that SOA, ammonia and nitrate had a higher fractional concentration during the haze episode than during the clean period, and ammonia concentration increased sharply at the onset of the haze.

However, compared to the measurement studies, SOSAA appears to have overestimated primary particle concentrations while underestimating SOA concentrations. Inorganics appear to be underestimated by SOSAA (10-15% of the mass modelled by SOSAA, compared to as much as 50% in the measurement studies), and sulfate is considerably underestimated (less than 3% of total mass modelled by SOSAA, compared to around 15% in the measurement studies during the episode). Cai et al. (2022) showed the

presence of wet aerosols during the haze episode. Therefore, the missing wet aerosol processes in the model (mentioned in section 2.3.4) may partly explain the significant underestimation of sulfate.

On November 15th, during the airmass shift, SOSAA showed a small peak in dust concentration, seen in Figure 10(b), which accounts for about 3% of the $PM_{0.84}$ mass. Otherwise, dust contributed to less than 1% of the PM mass throughout the study period. Thus, we conclude that dust did not significantly contribute to the observed haze during our case study. This agrees with the Cai et al. (2022) and Shen et al. (2020) measurement studies.

Figure 10(b-d) shows that the aerosols were older during the haze episode, with as much as 1/3 of the primary and SOA mass being more than two days old. Conversely, during the non-haze period, almost all of the primary and SOA mass was less than one day old.

Returning to the trajectory analysis, we next looked at the age of primary and SOA mass along the trajectories. Figure 11 shows the same example trajectories as in Figure 6, with the first three arriving during the haze episode and the last one arriving during the non-haze period after the episode. The panels on the left show the fraction of primary mass colored by the day of emission, and the panels on the right show the fraction of SOA mass colored by the day of formation. The percentages overlayed on the figure indicate the percentage of mass from each day that ultimately arrived at the station.

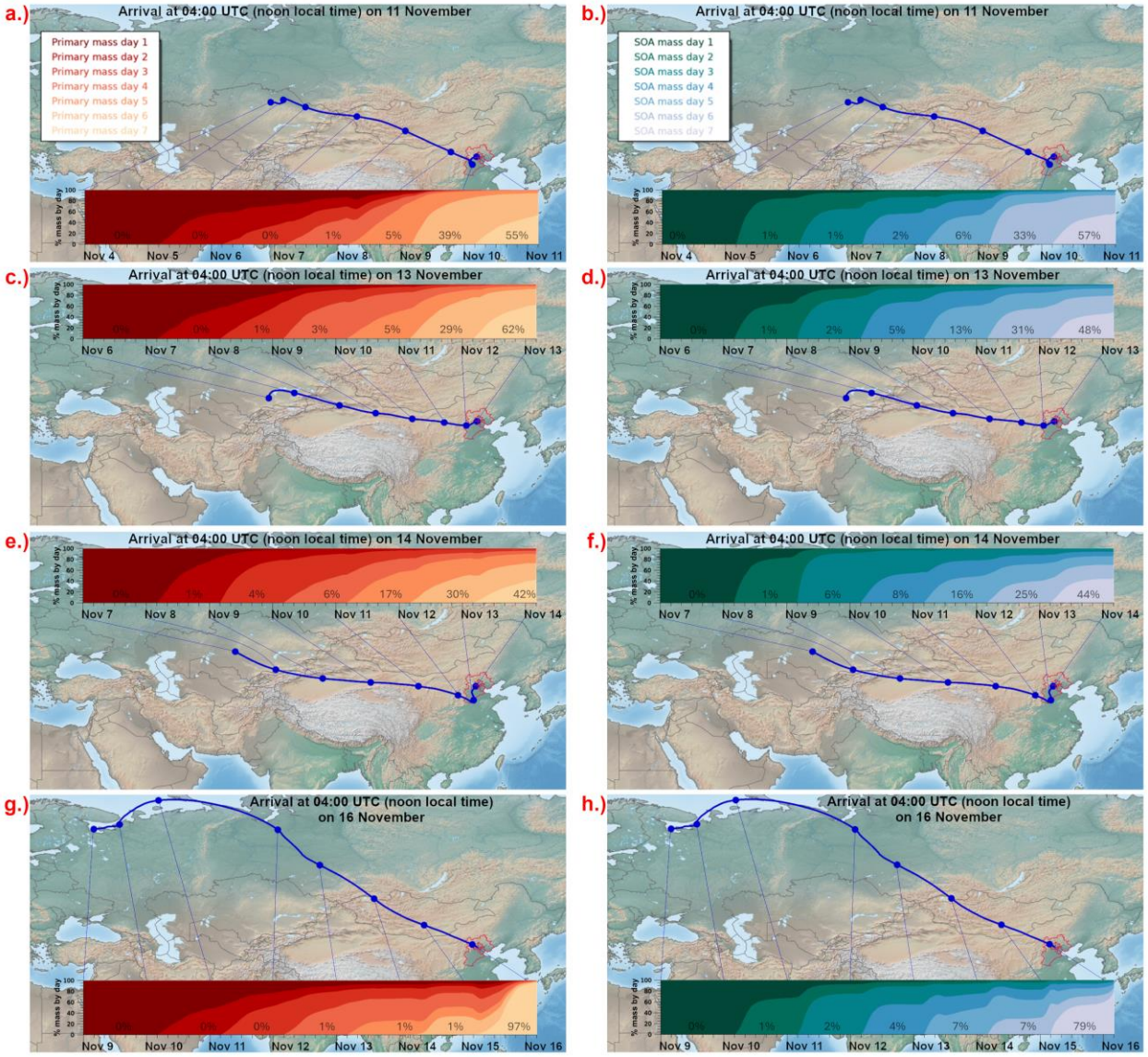

Fig. 11 Along-trajectory figures for the same arrival times shown in Figure 6. (a), (c), (e) and (g) show the fraction of primary particle mass emitted per day; and (b), (d), (f) and (h) show the fraction of SOA formed per day. The percentages along the bottom indicate the fraction of primary and SOA mass from the given day that arrived at the station. The BTH region is outlined in red.

We can see in Figure 11(a-b) that in the early stages of the haze episode, the BTH region contributed to over 60% of the primary and secondary mass. As the episode progressed, more PM was transported from outside the BTH region. Thus, a greater fraction of the mass originated from outside the BTH region rather than inside, and Figure 11(c-f) shows that during the heaviest part of the episode, more than half of the primary and SOA mass was transported from outside of the BTH area. This means that while the contribution of emission sources in the BTH region was certainly a significant contributor to the haze observed in Beijing, there was also a significant portion of emissions outside of this area that contributed to forming the haze that was transported into the city. On 14 November, shown in Figure 11 (e-f), 5% of the primary particle mass and 7% of the SOA mass originated in the Xinjiang region of western China.

This agrees with Lu et al. (2023), which found that secondary $PM_{2.5}$ was transported longer distances than primary $PM_{2.5}$.

Figure 11 (g-h) demonstrates the dramatically increasing contribution of nearby sources when cleaner airmasses from the northwest arrived at the NCP, as 97% of the primary mass and 79% of SOA mass were less than one day old. This resulted in the much different composition seen in Figure 10(b) on 16 November.

From this analysis, we conclude that local emission sources were the most significant contributors to air quality during the non-haze period. During the haze episode, however, there was a mix of local, regional, and long-range air pollution sources that contributed to the poor air quality.

4.5. Particle modes

After investigating the PNSD and the particle mass and age, we split the particle number concentration into three size modes: nucleation mode (<30 nm diameter), Aitken mode (30-100 nm), and accumulation mode (>100 nm). This is useful from a health standpoint because the smallest particles, especially particles in the Aitken mode size range, substantially impact health (Li et al., 2016; Han et al., 2016; Kwon et al., 2020). On the other hand, larger particles have the most influence on mass concentration (e.g., reported PM values). Thus, it is useful to look at the different size ranges individually. The time series of particle number concentrations in nucleation, Aitken, and accumulation modes are shown in Figure 12, along with DMPS measurements of number concentration in the same size ranges.

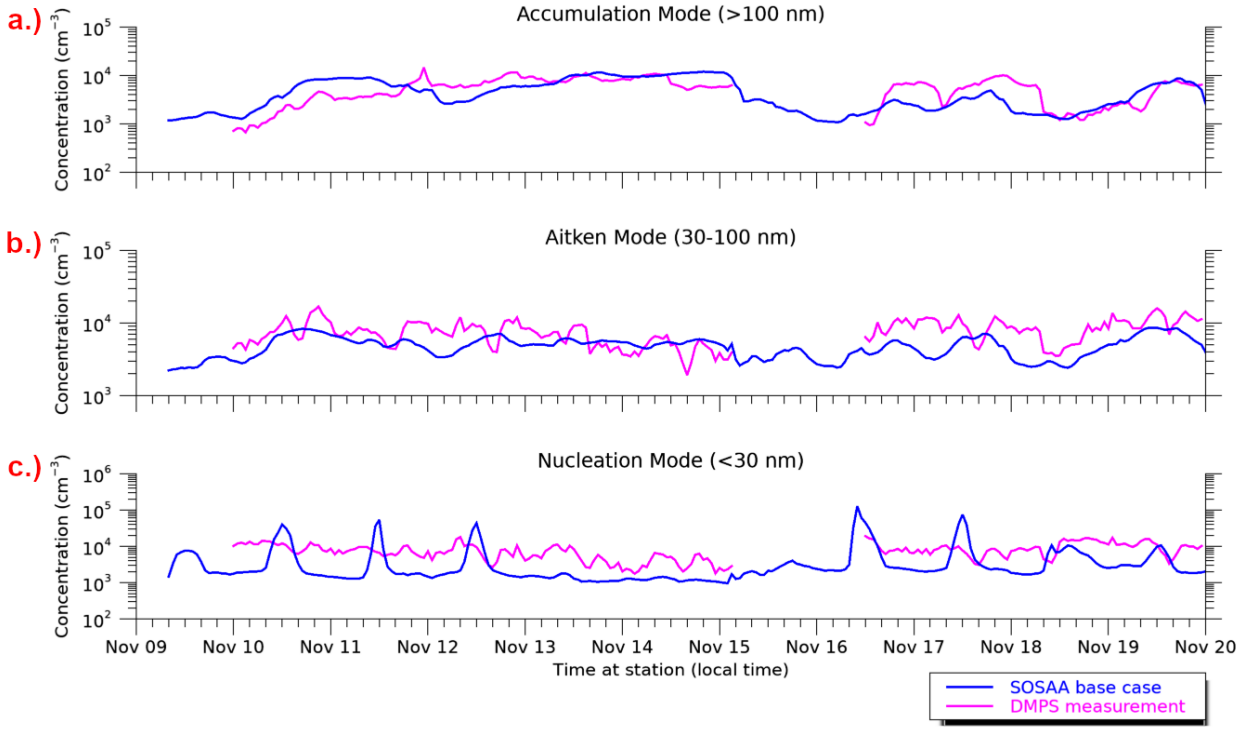

Fig. 12 Total particle number concentrations split into accumulation mode (a), Aitken mode (b), and nucleation mode (c) compared to DMPS measurements at BUCT-AHL

Figure 12 shows that SOSAA underestimates nucleation mode particles, except during some of the cases of midday NPF when SOSAA shows spikes in nucleation mode particles. Interestingly, the spikes in nucleation mode particles during NPF events are not clearly noticeable in the measurements in Figure 12(c). One explanation for this could be that there are many very localized emissions near the BUCT station, such as the nearby roads and the ring highway. Figure 12 shows reasonable agreement between the model and measurements for Aitken mode particles, and in general there is agreement between the model and measurements for accumulation mode particles, except during the buildup portion and the very last day of the haze episode, as previously noted. Overall, this is consistent with the model–measurement differences shown in Figure 8.

4.6. Time series of gas pollutants at BUCT-AHL

In addition to particle mass and number concentrations during the haze episode, we also looked at the results of pollutant gases modelled by SOSAA. The MCM chemistry scheme in SOSAA includes hundreds of gaseous compounds, and Figure 13 shows an example of a few selected ones. Specifically, we compared NO_x, SO_2, and carbon monoxide to the measurements at BUCT. We also looked at toluene and benzene and the toluene/benzene (T/B) ratio.

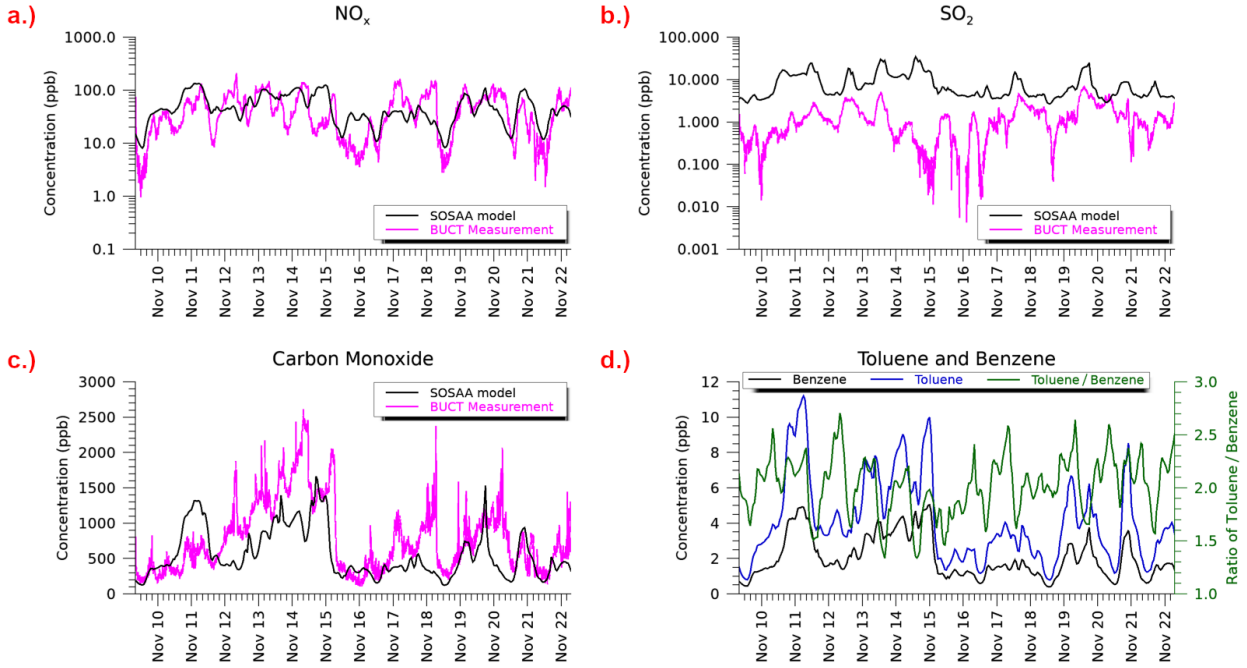

Fig. 13 Time series of some gas pollutants at BUCT-AHL simulated by SOSAA

The model reproduced the NO_x and CO measurements reasonably well, which will be investigated with statistical analysis in the next section. The model overestimates SO_2 concentrations. As mentioned in Section 2.3.4, SOSAA is already known to overestimate SO_2, likely because the model does not yet include cloud processes, which could be a major sink of SO_2. This is a component of SOSAA that is currently under development.

Previous studies by Ni et al. (2018) and He et al. (2012), have shown a similar overestimation of SO_2 in the WRF-Chem and CMAQ models, respectively. This overestimation in the models may also be because of uncertainties in the emission inventories, potentially related to the rapid decrease in SO_2 emissions in China over the past few decades, which may also affect the SOSAA results.

The T/B ratio is considered an indicator of emission source. When traffic is a heavy influence on emissions, ~1 < T/B < ~3, and a higher ratio is associated with solvent use and industrial processes (Cui et al., 2022; Tiwari et al., 2010; Zhang et al., 2015; Barletta et al., 2005). The T/B ratio modelled by SOSAA, shown in Figure 13(d), remains between 1 and 3 during the entire study period, indicating that traffic is likely the dominant source of emissions influencing the level of aromatic pollutants in Beijing. This result is consistent with Barletta et al. (2005).

4.7. Model Performance

We compared the base case to hourly averages of measurements at BUCT-AHL for $PM_{0.84}$, NO_2, NO_x, SO_2, and CO and plotted the MFE against MFB in the soccer goal plot in Figure 14. Each variable is plotted with three points: the squares represent all times, the triangles represent the analysis done using only data during the haze period, and the circles represent the analysis using only data during the non-haze period.

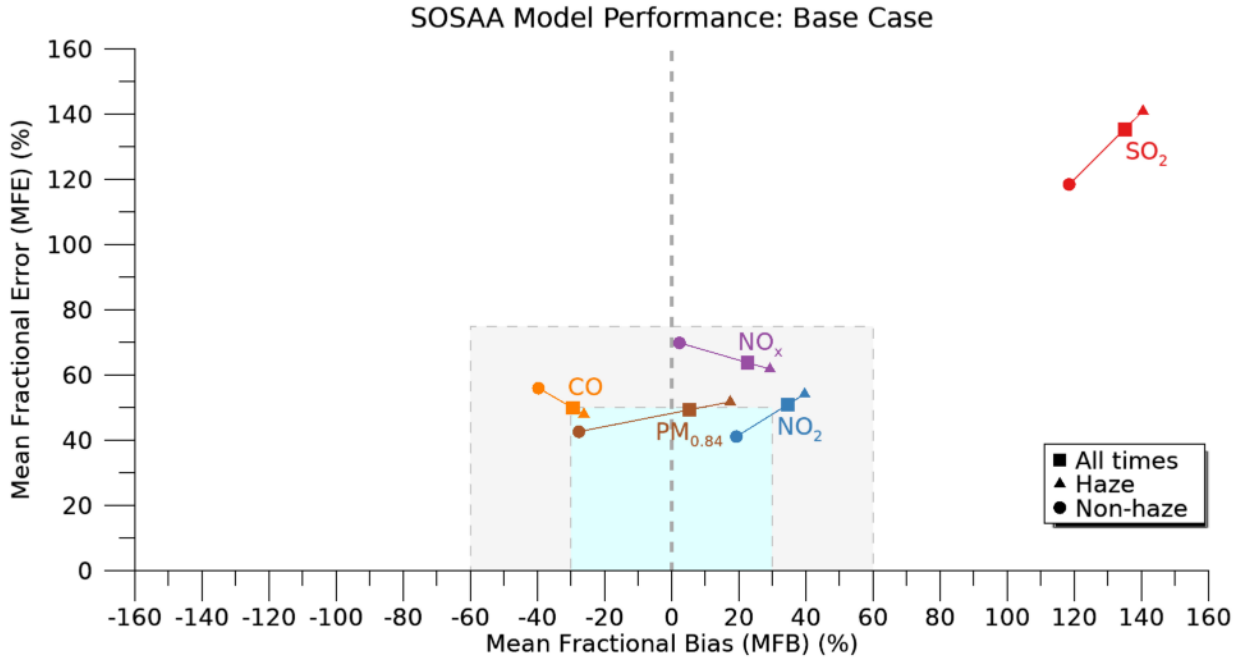

Fig. 14 Soccer goal plot showing SOSAA model performance of the base case compared to the measurements at BUCT-AHL. The benchmark criteria area (grey box) is where |MFB| < 60% and MFE < 75%, and the goal area (blue box) is where |MFB| < 30% and MFE < 50%

Again, the model overestimates SO_2 concentrations, which stands out in Figure 14. All other compounds compared are within the benchmark criteria defined in EPA (2007), meaning the model effectively represents the observed data during this case study.

Previous studies have indicated that regional air quality models generally underestimate PM and gas pollutants, especially during haze events (Zhai et al., 2024; Saide et al., 2020; Gao et al., 2022; Sokhi et al., 2022). However, Figure 14 shows that for SOSAA, the MFB is always a higher value (more positive or less negative, which is farther right on this figure), during the haze compared to non-haze for all pollutants, meaning that with respect to the measurements, SOSAA estimates higher during the haze period compared to the non-haze period.

5. Scenario analysis and sensitivity tests

After evaluating the model performance versus the measurements for the base case, we analyzed the scenarios and sensitivity tests, which were listed in Table 1 and described in detail in Section 2.5. First, we looked at the three scenarios from Section 2.5.1 (electric cars in the BTH region, comprehensive emission control in the BTH region, and comprehensive emission control only in Beijing), along with the zero anthropogenic emissions in Beijing and zero AWB test cases. These are plotted in Figure 15. In this figure, we further divided the particle number concentration into the three modes, like in Figure 12, but this time we show the percent change in number concentration for each of the three scenarios compared to the base case.

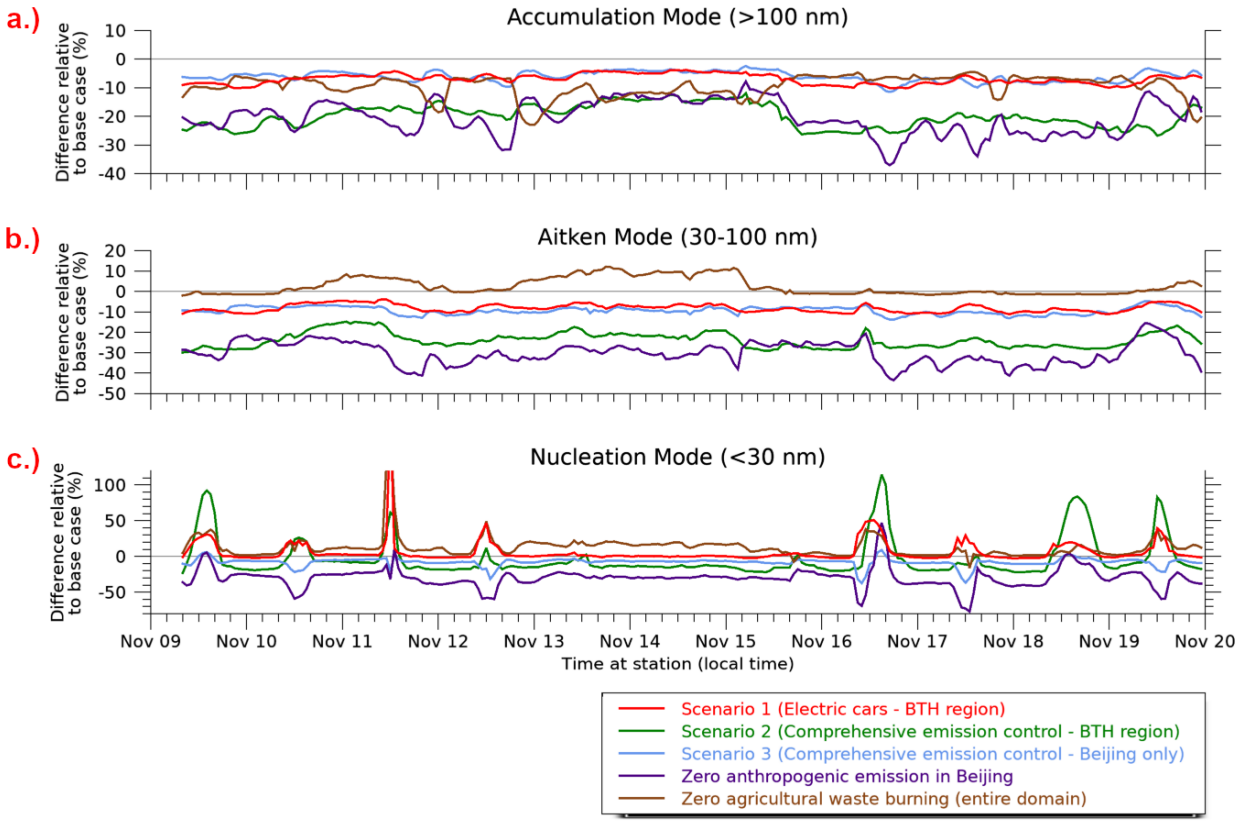

Fig. 15 Percent reduction in concentrations of nucleation mode, Aitken mode, and accumulation mode particles for the three scenarios, relative to the base case

In Figure 15, we see that Scenario 2 and the case of zero anthropogenic emissions in Beijing had the most significant particle reduction for all three modes. The case of zero emissions in Beijing had a bigger reduction during the non-haze time than the haze time, in agreement with the conclusion made at the end of section 4.4, that local emissions play a bigger role during non-haze, and regional and long-range sources are more significant during haze. Scenarios 1 and 2 only slightly reduced accumulation mode and Aitken mode particles, but these scenarios did not make a noticeable difference for nucleation mode particles. Eliminating AWB reduced accumulation mode particles, especially during the haze episode, but it increased Aitken mode and nucleation mode particles. We see an increase in NPF in the reduced emissions cases, evidenced by a spike in the nucleation mode number concentration. This is especially noticeable during the NPF event on November 16.

Next, we used the Mann-Whitney test for these three scenarios and two test cases to determine whether the tests improved air quality. The results of this test are described in the sections below and are also visualized in Figure S14 in the supplementary material.

It's important to note that the scenario results and sensitivity analysis for only one haze episode are not intended to inform decisions on emission control strategy. Rather, the results from these scenarios and tests offer some hints for how haze episodes could be mitigated and serve as a starting point for future, more detailed investigations.

5.1. Modified emissions scenarios

	Scenario 1 25% electric cars, BTH region	**Scenario 2** Comprehensive emission controls, BTH region	**Scenario 3** Comprehensive emission controls, Beijing city only
Improvement during haze episode:			
Accumulation mode	6%	19%	6%
Aitken mode	8%	23%	9%
Nucleation mode	No reduction	1%	7%
TOTAL PARTICLES	**4%**	**16%**	**7%**
Improvement during non-haze period:			
Accumulation mode	8%	22%	7%
Aitken mode	9%	27%	10%
Nucleation mode	No reduction	7%	10%
TOTAL PARTICLES	**3%**	**18%**	**10%**

Table 3 Comparative reduction of particle number concentration in the three modified emissions scenarios with respect to the base case

We see in Table 3 that Scenario 1 (electric cars in the BTH region) slightly reduced the number concentrations for Aitken mode and accumulation mode but not for nucleation mode particles. This scenario did not offer a statistically significant improvement to $PM_{0.84}$ or SO_2. Scenario 1 did, however, reduce NO_x and CO concentrations with statistical significance. Thus, we conclude that the transition to 25% electric vehicles, without any other emission control strategy, offers only marginal improvement in air quality.

Scenario 2 (comprehensive emission control in the BTH region) considerably reduced Aitken and accumulation mode particles, but it hardly reduced nucleation mode particle concentrations. This is because when overall concentrations are reduced, thus reducing CS, there is consequently an increase in NPF and, therefore, an increase in nucleation mode particles. $PM_{0.84}$ and gas pollutant concentrations were reduced in Scenario 2, with statistical significance.

Scenario 3 (comprehensive emission control only in Beijing) offered some reduction to particle number concentration in all three modes, but it did not reduce total $PM_{0.84}$ with statistical significance. This scenario reduced gas pollutant concentrations with statistical confidence, though the reduction was less than Scenario 2.

Overall, we conclude that regional emission control significantly improved air quality in this case study compared to only city-wide emission control.

5.2. Sensitivity to eliminating all anthropogenic emissions in Beijing

Although this is not necessarily a realistic emission reduction scenario, we can learn a couple of things from this sensitivity test. First, by taking the difference between the base case and this case, we can use it to estimate what fraction of particles was transported from outside the city versus emitted inside the city or formed by gas precursors that were emitted within the city (it is still possible that gas precursors were emitted outside the city, transported into the city, and then secondary particles formed within the city). The fractional reduction of particle number concentration for this sensitivity test is shown in Table 4.

	No emissions in Beijing Anthropogenic emission in the city removed from the model.
	Reduction during haze episode:
Accumulation mode	19%
Aitken mode	29%
Nucleation mode	29%
TOTAL PARTICLES	**23%**
	Reduction during clean period:
Accumulation mode	24%
Aitken mode	32%
Nucleation mode	32%
TOTAL PARTICLES	**30%**

Table 4 Comparative improvement of particle number concentration in the test case with zero anthropogenic emissions in the city of Beijing

In this sensitivity test, NO_x, SO_2, and CO were considerably reduced with statistical significance. The reduction was even more than in the three previous scenarios. However, this sensitivity test did not eliminate the haze in Beijing. Based on the SOSAA model, 77% of the particles during the haze episode and 70% during the non-haze period originated outside the city.

In other words, even if all emission sources in the city were shut off, the particle number concentrations wouldn't be reduced by more than 30%. This further demonstrates the importance of regional/provincial emission control measures rather than addressing air quality problems only at a city level, and it also demonstrates the need for cooperation between local and provincial or national regulatory authorities when making decisions on air quality policy, rather than individual cities working by themselves to address air quality problems.

The second thing we learned is that even though NPF was reduced in the city in this sensitivity test, NPF still occurred either in the city or immediately outside the city, which produced nucleation mode particles. This further illustrates that when the CS is reduced, conditions for NPF become more favorable. Therefore, the result from this sensitivity test demonstrates that as emissions are reduced over time, there will also be a need to focus on reducing NPF to prevent an increase in hazardous small particles in the atmosphere as an unintended consequence of emission reduction strategy.

5.3. Sensitivity to eliminating agricultural waste burning (AWB)

When AWB was removed from the model domain, accumulation mode particle concentration was reduced by 10% during the episode and 7% during the non-haze time. However, nucleation and Aitken mode particle concentrations were increased by eliminating AWB. This is likely because AWB emits mostly coarse particles, with the highest emissions in the GAINS dataset's 100-200 nm size bin. Consequently, by reducing the CS for gases, there was more NPF and more small particles. There is also less coagulation of particles as a result of reducing large particle concentrations. Increasing Aitken and nucleation mode particles is an unintended consequence of reducing emissions.

Eliminating AWB had a statistically significant reduction in PM mass but did not affect gas concentrations. Although there was some carbon monoxide emission from AWB, after investigating the CAMS datasets, we found that the emissions of CO from AWB are 2-3 orders of magnitude smaller than traffic, industry, and residential sources. Thus, the reduction is nearly negligible. Therefore, reducing AWB would reduce particle pollution during haze episodes but would likely not improve gas pollution or SOA concentrations.

This sensitivity test demonstrates that air quality in Beijing is a complicated system with many components and atmospheric processes interacting with each other. Like the electric cars scenario, reducing AWB would probably be more effective when combined with other emission reduction strategies.

One potential emission control strategy is to put burning restrictions into place if a haze episode is forecasted. These restrictions could prohibit AWB in areas forecasted to be upwind of major cities. In those areas, the post-harvest burning could be postponed until a time when haze is not predicted or when forecasted conditions are favorable for the emissions to be transported away from populated areas.

5.4. Sensitivity to different meteorological input data

For all the tested variables, using ERA5 meteorological dataset as input to FLEXPART and SOSAA resulted in statistically significant higher concentrations compared to the base case (which used Enviro-HIRLAM CAE input), based on the Mann-Whitney test. For $PM_{0.84}$, $Z = 8.97$ ($1–p = 1$).

When creating the same soccer goal plot from Section 4.7 (Figure 14), but using ERA5 as input, CO, NO_2, and NO_x fell within the criteria area, as shown in Figure 16(b). SO_2 was similarly overestimated by SOSAA. In this case, the biggest difference is that the $PM_{0.84}$ for the haze period was outside of the criteria area. Therefore, we conclude that for simulating PM concentration, the high-resolution Enviro-HIRLAM meteorology was more suitable for our case study rather than ERA5, especially for simulating haze.

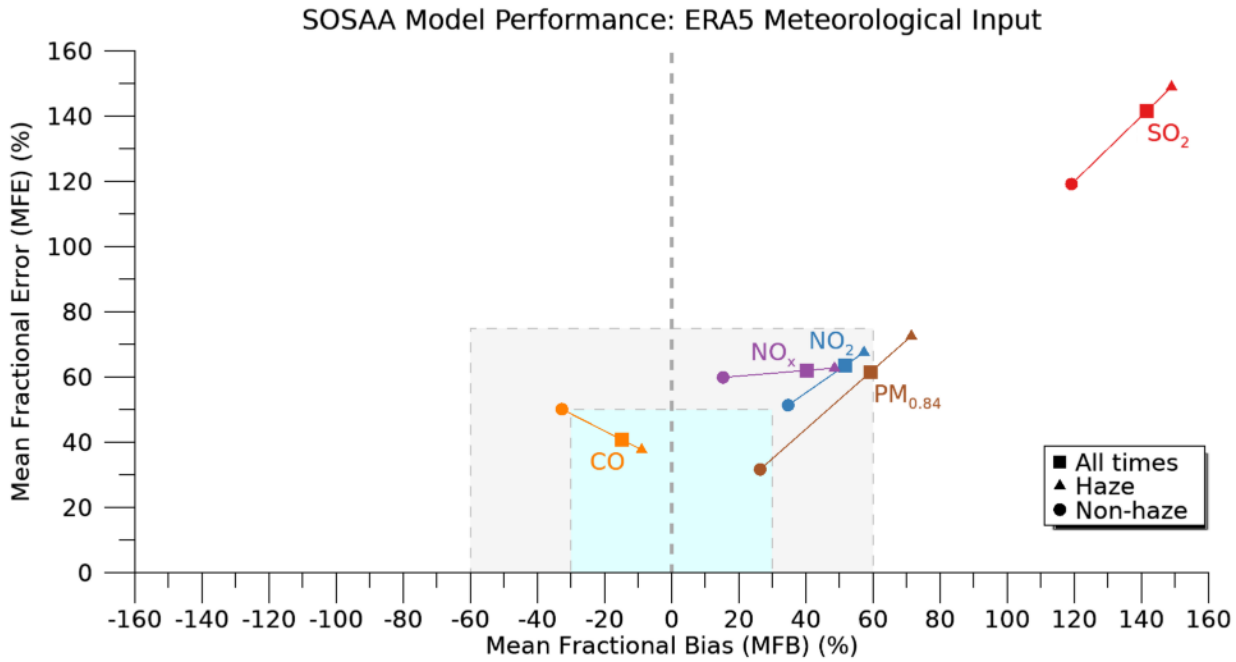

Fig. 16 Soccer goal plot ERA5 meteorology as input to FLEXPART and SOSAA

We also evaluated the results of SOSAA when using Enviro-HIRLAM DAE, IAE and NAE meteorology output as the input to FLEXPART-SOSAA, in comparison to the base case (with Enviro-HIRLAM CAE). We found that there was no statistically significant difference between SOSAA results obtained when using output from different Enviro-HIRLAM runs as input to FLEXPART-SOSAA.

5.5. Sensitivity to increased VOCs

Our final sensitivity test involved doubling VOC (both anthropogenic and biogenic) emissions throughout the entire model domain. As seen in Figure 17, this made very little difference during the haze episode because the CS is already so high, meaning that gases condense directly onto the preexisting large particles rather than form new particles and grow. Nonetheless, we see that there is somewhat stronger NPF in the double VOC case, even though the particles that are formed don't subsequently grow. The biggest difference in this sensitivity test is at the beginning of the haze episode and during the non-haze period, notably on November 9, 16 and 18, when the NPF events and subsequent particle growth are much stronger in the double VOC case.

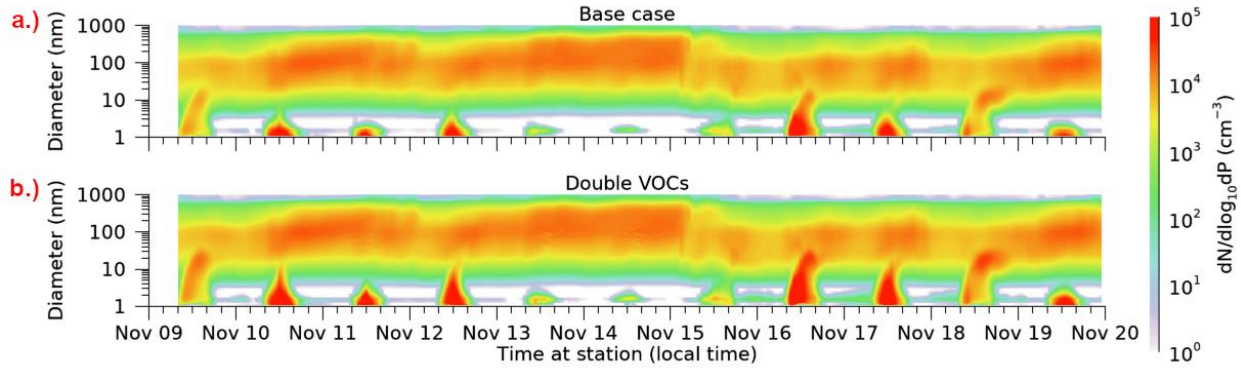

Fig. 17 Result of sensitivity test where VOC emissions were doubled throughout the model domain

Despite increased nucleation and particle growth during the non-haze period, the resulting PM mass showed little change with the addition of more VOCs. Statistical analysis revealed no significant difference in PM mass or gas concentrations between the base case and the double VOC case. This result is not surprising, given that larger-sized particles dominate PM mass. However, there was increased growth of nucleation and Aitken mode particles. This observation is important in terms of atmospheric chemical and physical processes, suggesting that future model development could focus on enhancing this area.

This sensitivity test highlights the importance of primary emissions and the relationship between primary and secondary aerosols. During the haze period marked by heavy aerosol loading, altering the VOCs without changing primary emissions results in minimal impact on the total PM mass. A comprehensive emission strategy that addresses both primary particle emissions and VOCs would be more effective than targeting one or the other.

6. Conclusions

This study demonstrated that SOSAA, which was run along trajectories arriving in Beijing during and a few days after a severe haze episode affected the region, was effective at modelling air quality. When comparing $PM_{0.84}$, CO, NO_2, and NO_x to measurements at BUCT-AHL during this case study, SOSAA met the criteria for a suitable model based on the 2007 EPA guidelines for model evaluation.

This study also showed that SOSAA is useful for determining the origins of haze measured in Beijing and ascertaining how potential changes to emissions would influence haze formation and chemical composition. Additionally, it outlined some potential improvements to the model and to modelling haze in general.

This study found that up to 77% of particles arriving in Beijing during the investigated haze episode originated outside the city and were transported into the city. The trajectory analysis showed that as much as 5% of the primary particle mass and 7% of SOA mass that arrived in Beijing during the peak of the haze episode originated in western China, as far as 2000 km west. In most of the trajectories, the accumulation of aerosol particle concentrations leading to haze began when the trajectories entered regions of northern and western China with heavy emissions.

The model showed that during this case study period, PM in Beijing was dominated by primary emissions. However, primary particles and SOA are key in Beijing's overall aerosol dynamics. Although the emission control scenarios we simulated showed an overall reduction in particle concentrations, new particle formation events, and thus, concentrations of small particles increased when particle concentrations were reduced. Thus, we conclude that reducing or eliminating primary emission without simultaneously reducing SOA precursors may have the unintended consequence of causing SOA to increase.

Scenario analysis showed some promising examples of how reducing emissions could improve air quality. We conclude that air quality mitigation strategy should focus on comprehensive control rather than just one source or sector. The strategy should also focus on regional or national policy rather than only the city of Beijing because focusing only on the city would likely make little difference in improving air quality.

Results also showed that eliminating agricultural waste burning could reduce haze particle concentrations, especially larger particles. Therefore, one potential haze mitigation strategy could be that if haze is forecasted, a ban on agricultural burning in Beijing’s forecasted upwind directions could be implemented. The burning could be postponed until a time when downwind haze is not in the forecast.

When testing different meteorological inputs to the FLEXPART-SOSAA modelling system for this selected haze episode in November 2018, Enviro-HIRLAM showed improved results over ERA5. However, during this case study, there was no statistically significant difference obtained between the different Enviro-HIRLAM runs (DAE, IAE, and NAE), compared to the base case (CAE).

Our results indicate that SOSAA overestimates SO_2, and processes currently under development, such as the particle phase chemistry module or updated emission databases, will likely improve the model. We also found that a potential improvement to the SOSAA model could be to more accurately simulate chemical mechanisms involving VOCs, especially aromatics, as these mechanisms currently may not be fully accounted for in the model.

In conclusion, this study demonstrated that SOSAA can simulate haze and air pollution in China. Our results highlight Beijing's complex air quality dynamics, particularly during severe haze episodes, and underscore the importance of using process-based modelling systems like SOSAA for effective air quality analysis. Our results demonstrate that emission control strategies must address multiple sectors and should simultaneously reduce primary emissions and SOA precursors for optimal results. Effective mitigation strategies should therefore adopt a comprehensive approach, emphasizing regional and national coordination. Overall, this study offers valuable tools for developing targeted, efficient air quality control strategies in Beijing and other heavily polluted urban areas.

Data Availability

For the Enviro-HIRLAM-FLEXPART integration project, please see the Data Availability statement in Foreback et al. (2024). The supplementary material of Foreback et al. (2024) also contains an example postprocessing script for Enviro-HIRLAM meteorological output for use as input for FLEXPART and SOSAA.

Output datasets of this project are available upon request from the authors. SOSAA model code will be made publicly available in the near future.

Funding

Funding for this project came in part from the Jenny and Antti Wihuri Foundation project, with the grant for "Air pollution cocktail in Gigacity." Funding was also received from the Research Council of Finland (formerly the Academy of Finland, AoF) projects 311932 and 360114 and flagship ACCC ("The Atmosphere and Climate Competence Center" under grant agreement No 337549) and applied towards this project. Partially, funding included contribution from EU Horizon 2020 projects CRiceS ("Climate relevant interactions and feedbacks: the key role of sea ice and snow in the polar and global climate system" under grant agreement No 101003826) and FORCeS (Constrained aerosol forcing for improved climate projections under grant agreement No 821205); and Horizon Europe project FOCI ("Non-CO2 Forcers and their Climate, Weather, Air Quality and Health Impacts" under grant agreement No 101056783). Additionally, internal funding at the University of Helsinki's Lahti University Campus was used for work on this project.

Competing interests

The authors declare that there are no known competing financial or personal interests which could have influenced this work.

References

Amann M, Bertok I, Borken-Kleefeld J, Cofala J, Heyes C, Höglund-Isaksson L, Klimont Z, Nguyen B, Posch M, Rafaj P, Sandler R, Schöpp W, Wagner F, Winiwarter W (2011). Cost-effective control of air quality and greenhouse gases in Europe: Modeling and policy applications. Environ Modell Softw 26 (12), 1489-1501. https://doi.org/10.1016/j.envsoft.2011.07.012

Baklanov A, Molina L, Gauss M (2016) Megacities, air quality and climate. Atmos Environ 126, 235-249. https://doi.org/10.1016/j.atmosenv.2015.11.059

Baklanov A, Smith Korsholm U, Nuterman R, Mahura A, Nielsen KP, Sass BH, Rasmussen A, Zakey A, Kaas E, Kurganskiy A, Sørensen B, González-Aparicio I (2017) Enviro-HIRLAM online integrated meteorology–chemistry modelling system: strategy, methodology, developments and applications (v7.2). Geosci Model Dev 10, 2971–2999. https://doi.org/10.5194/gmd-10-2971-2017

Barletta B, Meinardi S, Rowland FS, Chan C-Y, Wang X, Zou S, Chan LY, Blake DR (2005) Volatile organic compounds in 43 Chinese cities. Atmos Environ 39:32, 5979-5990. https://doi.org/10.1016/j.atmosenv.2005.06.029

Besel V, Kubečka J, Kurtén T, Vehkamäki H (2020) Impact of Quantum Chemistry Parameter Choices and Cluster Distribution Model Settings on Modeled Atmospheric Particle Formation Rates. J Phys Chem A 124 (28), 5931-5943. https://doi.org/10.1021/acs.jpca.0c03984

Bloss C, Wagner V, Jenkin ME, Volkamer R, Bloss WJ, Lee JD, Heard DE, Wirtz K, Martin-Reviejo M, Rea G, Wenger JC, Pilling MJ (2005) Development of a detailed chemical mechanism (MCMv3.1) for the atmospheric oxidation of aromatic hydrocarbons. Atmos Chem Phys 5, 641–664. https://doi.org/10.5194/acp-5-641-2005

Boy M, Sogachev A, Lauros J, Zhou L, Guenther A, Smolander S (2011) SOSA – a new model to simulate the concentrations of organic vapours and sulphuric acid inside the ABL – Part 1: Model description and initial evaluation. Atmos Chem Phys 11, 43–51. https://doi.org/10.5194/acp-11-43-2011

Cai J, Wu C, Wang J, Du W, Zheng F, Hakala S, Fan X, Chu B, Yao L, Feng Z, Liu Y, Sun Y, Zheng J, Yan C, Bianchi F, Kulmala M, Mohr C, Daellenbach KR (2022) Influence of organic aerosol molecular composition on particle absorptive properties in autumn Beijing. Atmos Chem Phys 22, 1251–1269. https://doi.org/10.5194/acp-22-1251-2022

Cai W, Li K, Liao H, Wang H, Wu L (2017) Weather conditions conducive to Beijing severe haze more frequent under climate change. Nat Clim Change 7, 257–262. https://doi.org/10.1038/nclimate3249

Cao J, Qiu X, Gao J, Wang F, Wang J, Wu J, Peng L (2021) Significant decrease in SO_2 emission and enhanced atmospheric oxidation trigger changes in sulfate formation pathways in China during 2008–2016. J Clean Prod 326, 129396. https://doi.org/10.1016/j.jclepro.2021.129396

Chen D, Xavier C, Clusius P, Nieminen T, Roldin P, Qi X, Pichelstorfer L, Kulmala M, Rantala P, Aalto J, Sarnela N, Kolari P, Keronen P, Rissanen M, Taipale D, Foreback B, Baykara M, Zhou P, Boy M (2021) A modelling study of OH, NO3 and H2SO4 in 2007–2018 at SMEAR II, Finland: analysis of long-term trends. Environmental Science: Atmospheres. https://doi.org/10.1039/D1EA00020A

Chen L, Zhu J, Liao H, Gao Y, Qiu Y, Zhang M, Liu Z, Li N, Wang Y (2019) Assessing the formation and evolution mechanisms of severe haze pollution in the Beijing–Tianjin–Hebei region using process analysis. Atmos Chem Phys 19, 10845–10864. https://doi.org/10.5194/acp-19-10845-2019

Cheng Y, Cao X, Liu J, Yu Q, Zhong Y, Geng G, Zhang Q, He K (2022) New open burning policy reshaped the aerosol characteristics of agricultural fire episodes in Northeast China. Sci Tot Environ 810 152272. https://doi.org/10.1016/j.scitotenv.2021.152272

Clusius P, Xavier C, Pichelstorfer L, Zhou P, Olenius T, Roldin P, Boy M (2022) Atmospherically Relevant Chemistry and Aerosol box model – ARCA box (version 1.2). Geosci Model Dev 15, 7257–7286. https://doi.org/10.5194/gmd-15-7257-2022

Cui L, Wu D, Wang S, Xu Q, Hu R, Hao J (2022) Measurement report: Ambient volatile organic compound (VOC) pollution in urban Beijing: characteristics, sources, and implications for pollution control. Atmos Chem Phys 22, 11931–11944. https://doi.org/10.5194/acp-22-11931-2022

Daellenbach KR, Cai J, Hakala S, Dada L, Yan C, Du W, Yao L, Zheng F, Ma J, Ungeheuer F, Vogel AL, Stolzenburg D, Hao Y, Liu Y, Bianchi F, Uzu G, Jaffrezo J-L, Worsnop DR, Donahue NM, Kulmala M (2024). Substantial contribution of transported emissions to organic aerosol in Beijing. Nat Geosci 17, 747–754. https://doi.org/10.1038/s41561-024-01493-3

Dang R, Liao H.: Severe winter haze days in the Beijing–Tianjin–Hebei region from 1985 to 2017 and the roles of anthropogenic emissions and meteorology. Atmos Chem Phys 19, 10801–10816. https://doi.org/10.5194/acp-19-10801-2019

Digital Typhoon (2024) Database of Weather Charts for Hundred Years - Archive of Weather Charts in the Past and the History of Japanese Meteorological Observations. http://agora.ex.nii.ac.jp/digital-typhoon/weather-chart/. Accessed 29 April 2024

Ding D, Jiang Y, Wang S, Xing J, Dong Z, Hao J, Paasonen P (2024). Unveiling the health impacts of air pollution transport in China. Environ Int 191, 108947. https://doi.org/10.1016/j.envint.2024.108947

Fang M, Chan CK, Yao X (2009) Managing air quality in a rapidly developing nation: China. Atmos Environ 43 (1), 79-86. https://doi.org/10.1016/j.atmosenv.2008.09.064

Foreback B, Mahura A, Clusius P, Xavier C, Baykara M, Zhou P, Nieminen T, Sinclair V, Kerminen V-M, Kokkonen T V, Hakala S, Aliaga D, Makkonen R, Baklanov A, Nuterman R, Xia M, Hua C, Liu Y, Kulmala M, Paasonen P, Boy M (2024) A new implementation of FLEXPART with Enviro-HIRLAM meteorological input, and a case study during a heavy air pollution event. Big Earth Data 8(2), 397–434. https://doi.org/10.1080/20964471.2024.2316320

Gao C, Xiu A, Zhang X, Tong Q, Zhao H, Zhang S, Yang G, Zhang M (2022) Two-way coupled meteorology and air quality models in Asia: a systematic review and meta-analysis of impacts of aerosol feedbacks on meteorology and air quality. Atmos Chem Phys 22, 5265–5329. https://doi.org/10.5194/acp-22-5265-2022

Gao M, Guttikunda SK, Carmichael GR, Wang Y, Liu Z, Stanier CO, Saide PE, Yu M (2015a) Health impacts and economic losses assessment of the 2013 severe haze event in Beijing area. Sci Total Environ 511, 553-561. https://doi.org/10.1016/j.scitotenv.2015.01.005

Gao Y, Zhang M, Liu Z, Wang L, Wang P, Xia X, Tao M, Zhu L (2015b) Modeling the feedback between aerosol and meteorological variables in the atmospheric boundary layer during a severe fog–haze event over the North China Plain. Atmos Chem Phys 15, 4279–4295. https://doi.org/10.5194/acp-15-4279-2015

Granier C, Darras S, van der Gon HD, Doubalova J, Elguindi N, Galle B, Gauss M, Guevara M, Jalkanen J-P, Kuenen J, Liousse C, Quack B, Simpson D, Sindelarova K (2019) The Copernicus Atmosphere Monitoring Service global and regional emissions (April 2019 version), Copernicus Atmosphere Monitoring Service (CAMS) report. https://doi.org/10.24380/d0bn-kx16

Guevara M, Jorba O, Tena C, Denier van der Gon H, Kuenen J, Elguindi N, Darras S, Granier C, Pérez García-Pando C (2020) Copernicus Atmosphere Monitoring Service TEMPOral profiles for the Global

domain version 21 (CAMS-GLOB-TEMPOv21). Copernicus Atmosphere Monitoring Service (CAMS) [publisher], ECCAD [distributor]. https://doi.org/10.24380/ks45-9147

Guevara M, Jorba O, Tena C, Denier van der Gon H, Kuenen J, Elguindi N, Darras S, Granier C, Pérez García-Pando C (2021) Copernicus Atmosphere Monitoring Service TEMPOral profiles (CAMS-TEMPO): global and European emission temporal profile maps for atmospheric chemistry modelling. Earth Syst Sci Data 13, 367–404. https://doi.org/10.5194/essd-13-367-2021

Hakala S, Vakkari V, Bianchi F, Dada L, Deng C, Dällenbach KR, Fu Y, Jiang J, Kangasluoma J, Kujansuu J, Liu Y, Petäjä T, Wang L, Yan C, Kulmala M, Paasonen P (2022) Observed coupling between air mass history, secondary growth of nucleation mode particles and aerosol pollution levels in Beijing. Environmental Science: Atmospheres 2, 146-164. https://doi.org/10.1039/D1EA00089F

Han Y, Zhu T, Guan T, Zhu Y, Liu J, Ji Y, Gao S, Wang F, Lu H, Huang W (2016) Association between size-segregated particles in ambient air and acute respiratory inflammation. Sci Total Environ 565, 412-419. https://doi.org/10.1016/j.scitotenv.2016.04.196

Hari P, Kulmala M (2005) Station for Measuring Ecosystem-Atmosphere Relations (SMEAR II). Boreal Environ Res 10(5), 315-322.

He H, Li C, Loughner CP, Li Z, Krotkov NA, Yang K, Wang L, Zheng Y, Bao X, Zhao G, Dickerson RR (2012) SO_2 over central China: Measurements, numerical simulations and the tropospheric sulfur budget. J Geophy Res-Atmos 117, 37–51. https://doi.org/10.1029/2011jd016473

Hersbach H, Bell B, Berrisford P, Hirahara S, Horányi A, Muñoz-Sabater J, Nicolas J, Peubey C, Radu R, Schepers D, Simmons A, Soci C, Abdalla S, Abellan X, Balsamo G, Bechtold P, Biavati G, Bidlot J et al (2020). The ERA5 global reanalysis. Q J Roy Meteor Soc 146(730), 1999–2049. https://doi.org/10.1002/qj.3803

Hess P, Kinnison D, Tang Q (2015) Ensemble simulations of the role of the stratosphere in the attribution of northern extratropical tropospheric ozone variability. Atmos Chem Phys 15, 2341–2365. https://doi.org/10.5194/acp-15-2341-2015

Hua Y, Wang S, Jiang J, Zhou W, Xu Q, Li X, Liu B, Zhang D, Zheng M (2018) Characteristics and sources of aerosol pollution at a polluted rural site southwest in Beijing, China. Sci Total Environ 626, 519-527. https://doi.org/10.1016/j.scitotenv.2018.01.047

Huang X, Liu Z, Liu J, Hu B, Wen T, Tang G, Zhang J, Wu F, Ji D, Wang L, Wang Y (2017) Chemical characterization and source identification of $PM_{2.5}$ at multiple sites in the Beijing–Tianjin–Hebei region, China. Atmos Chem Phys 17, 12941–12962. https://doi.org/10.5194/acp-17-12941-2017

Inness A, Ades M, Agustí-Panareda A, Barré J, Benedictow A, Blechschmidt A-M, Dominguez JJ, Engelen R, Eskes H, Flemming J, Huijnen V, Jones L, Kipling Z, Massart S, Parrington M, Peuch V-H, Razinger M, Remy S, Schulz M, Suttie M (2019) The CAMS reanalysis of atmospheric composition. Atmos Chem Phys 19, 3515–3556. https://doi.org/10.5194/acp-19-3515-2019

Jalkanen J-P, Johansson L, Kukkonen J, Brink A, Kalli J, Stipa T (2012) Extension of an assessment model of ship traffic exhaust emissions for particulate matter and carbon monoxide. Atmos Chem Phys 2641-2659. https://doi.org/10.5194/acp-12-2641-2012

Jalkanen J-P, Johansson L, Kukkonen J (2016) A comprehensive inventory of ship traffic exhaust emissions in the European sea areas in 2011. Atmos Chem Phys 71-84. https://doi.org/10.5194/acp-16-71-2016

Jenkin ME, Saunders SM, Pilling MJ (1997) The tropospheric degradation of volatile organic compounds: a protocol for mechanism development. Atmos Environ 31,1: 81–104. https://doi.org/10.1016/S1352-2310(96)00105-7

Jenkin ME, Saunders SM, Wagner V, Pilling MJ (2003) Protocol for the development of the Master Chemical Mechanism, MCM v3 (Part B): tropospheric degradation of aromatic volatile organic compounds. Atmos Chem Phys 3, 181–193. https://doi.org/10.5194/acp-3-181-2003

Jenkin ME, Wyche KP, Evans CJ, Carr T, Monks PS, Alfarra MR, Barley MH, McFiggans GB, Young JC, Rickard AR (2012) Development and chamber evaluation of the MCM v3.2 degradation scheme for β-caryophyllene. Atmos Chem Phys 12, 5275–5308. https://doi.org/10.5194/acp-12-5275-2012

Jenkin ME, Young JC, Rickard AR. (2015) The MCM v3.3.1 degradation scheme for isoprene. Atmos Chem Phys 15, 11433–11459. https://doi.org/10.5194/acp-15-11433-2015

Ji D, Wang Y, Wang L, Chen L, Hu B, Tang G, Xin J, Song T, Wen T, Sun Y, Pan Y, Liu Z (2012) Analysis of heavy pollution episodes in selected cities of northern China. Atmos Environ 50, 338-348. https://doi.org/10.1016/j.atmosenv.2011.11.053

Jiang J, Zhou W, Cheng Z, Wang S, He K, Hao J (2015) Particulate Matter Distributions in China during a Winter Period with Frequent Pollution Episodes (January 2013). Aerosol Air Qual Res 15, 494-503. https://doi.org/10.4209/aaqr.2014.04.0070

Jiang Y, Liang X, Zhang S, Hu Z, Hove A, Wu Y (2023) The future air quality impact of electric vehicle promotion and coordinated charging in the Beijing-Tianjin-Hebei region. Environ Pollut 332, 121928. https://doi.org/10.1016/j.envpol.2023.121928

Johansson L, Jalkanen J-P, Kalli J, Kukkonen J (2013) The evolution of shipping emissions and the costs of regulation changes in the northern EU area. Atmos Chem Phys 13, 11375–11389. https://doi.org/10.5194/acp-13-11375-2013

Johansson L, Jalkanen J-P, Kukkonen J (2017) Global assessment of shipping emissions in 2015 on a high spatial and temporal resolution. Atmos Environ 167, 403-415. https://doi.org/10.1016/j.atmosenv.2017.08.042

Kok JF, Mahowald NM, Fratini G, Gillies JA, Ishizuka M, Leys JF, Mikami M, Park M-S, Park S-U, Van Pelt RS, Zobeck TM (2014) An improved dust emission model – Part 1: Model description and comparison against measurements. Atmos Chem Phys 14, 13023–13041. https://doi.org/10.5194/acp-14-13023-2014

Korsholm US, Mahura A, Baklanov A, Grell G (2010) Interactions between Air Quality and Meteorology/Climate: Aerosol Feedbacks, in: FP7 MEGAPOLI Sci Report, edited by: Baklanov, A. and Mahura, A. 10-10, 31–46.

Kulmala M (2015) Atmospheric chemistry: China's choking cocktail. Nature 526, 497–499. https://doi.org/10.1038/526497a

Kulmala M (2018) Build a global Earth observatory. Nature 553, 21–23. https://doi.org/10.1038/d41586-017-08967-y

Kumar P, Morawska L, Martani C, Biskos G, Neophytou M, Di Sabatino S, Bell M, Norford L, Britter R (2015) The rise of low-cost sensing for managing air pollution in cities. Environ Int 75, 199-205. https://doi.org/10.1016/j.envint.2014.11.019

Kwon HS, Ryu MH, Carlsten C (2020) Ultrafine particles: unique physicochemical properties relevant to health and disease. Exp Mol Med 52, 318–328. https://doi.org/10.1038/s12276-020-0405-1

Lana A, Bell TG, Simo R, Vallina SM, Ballabrera-Poy J, Kettle AJ, Dachs J, Bopp L, Saltzman ES, Stefels J, Johnson JE, Liss PS (2011) An updated climatology of surface dimethlysulfide concentrations and emission fluxes in the global ocean. Global Biogeochem Cy 25, 17. https://doi.org/10.1029/2010GB003850

Lennartz ST, Marandino CA, von Hobe M, Cortes P, Quack B, Simo R, Booge D, Pozzer A, Steinhoff T, Arevalo-Martinez DL, Kloss C, Bracher A, Röttgers R, Atlas E, Krüger K (2017) Direct oceanic emissions unlikely to account for the missing source of atmospheric carbonyl sulfide. Atmos Chem Phys 17, 385–402. https://doi.org/10.5194/acp-17-385-2017

Leung DM, Kok JF, Li L, Okin GS, Prigent C, Klose M, Pérez García-Pando C, Menut L, Mahowald NM, Lawrence DM, Chamecki M (2023) A new process-based and scale-aware desert dust emission scheme for global climate models – Part I: Description and evaluation against inverse modeling emissions. Atmos Chem Phys 23, 6487–6523. https://doi.org/10.5194/acp-23-6487-2023

Li X, Yan C, Patterson RF, Zhu Y, Yao X, Zhu Y, Ma S, Qiu X, Zhu T, Zheng M (2016) Modeled deposition of fine particles in human airway in Beijing, China. Atmos Environ 124(B), 387-395. https://doi.org/10.1016/j.atmosenv.2015.06.045

Liu J, Gao Z, Wang L, Li Y, Gao CY (2018a) The impact of urbanization on wind speed and surface aerodynamic characteristics in Beijing during 1991–2011. Meteorol Atmos Phys 130, 311–324. https://doi.org/10.1007/s00703-017-0519-8

Liu J, Chen Y, Chao S, Cao H, Zhang A (2019). Levels and health risks of $PM_{2.5}$-bound toxic metals from firework/firecracker burning during festival periods in response to management strategies. Ecotox Environ Safe 171, 406–413. https://doi.org/10.1016/j.ecoenv.2018.12.104

Liu P, Ye C, Xue C, Zhang C, Mu Y, Sun X (2020a) Formation mechanisms of atmospheric nitrate and sulfate during the winter haze pollution periods in Beijing: gas-phase, heterogeneous and aqueous-phase chemistry Atmos Chem Phys 20, 4153–4165. https://doi.org/10.5194/acp-20-4153-2020

Liu Q, Jia X, Quan J, Li J, Li X, Wu Y, Chen D, Wang Z, Liu Y (2018b) New positive feedback mechanism between boundary layer meteorology and secondary aerosol formation during severe haze events. Sci Rep 8, 6095. https://doi.org/10.1038/s41598-018-24366-3

Liu T, Chan AWH, Abbatt JPD (2021) Multiphase Oxidation of Sulfur Dioxide in Aerosol Particles: Implications for Sulfate Formation in Polluted Environments. Environ Sci Technol 55:8, 4227–4242. https://doi.org/10.1021/acs.est.0c06496

Liu XG, Li J, Qu Y, Han T, Hou L, Gu J, Chen C, Yang Y, Liu X, Yang T, Zhang Y, Tian H, Hu M (2013). Formation and evolution mechanism of regional haze: a case study in the megacity Beijing, China. Atmos Chem Phys 13, 4501–4514. https://doi.org/10.5194/acp-13-4501-2013

Liu YC, Yan C, Feng Z, Zheng F, Fan X, Zhang Y, Li C, Zhou Y, Lin Z, Guo Y, Zhang Y, Ma L, Zhou W, Liu Z, Dada L, Dällenbach K, Kontkanen J, Cai R, Chan T, Chu B, Du W, Yao L, Wang Y, Cai J, Kangasluoma J, Kokkonen T, Kujansuu J, Rusanen A, Deng C, Fu Y, Yin R, Li X, Lu Y, Liu Y, Lian C, Yang D, Wang W, Ge M, Wang Y, Worsnop DR, Junninen H, He H, Kerminen V-M, Zheng J, Wang L, Jiang J, Petäjä T, Bianchi F, Kulmala M (2020b) Continuous and comprehensive atmospheric observation in Beijing: a station to understand the complex urban atmospheric environment. Big Earth Data 4, 295-321. https://doi.org/10.1080/20964471.2020.1798707

Lu P, Deng S, Li G, Tuheti A, Liu J (2023) Regional Transport of $PM_{2.5}$ from Coal-Fired Power Plants in the Fenwei Plain, China. Int J Env Res Pub He 20(3), 2170. https://doi.org/10.3390/ijerph20032170

Luo M, Ji Y, Ren Y, Gao F, Zhang H, Zhang L, Yu Y, Li H (2021) Characteristics and Health Risk Assessment of $PM_{2.5}$-Bound PAHs during Heavy Air Pollution Episodes in Winter in Urban Area of Beijing, China. Atmosphere 12(3), 323. https://doi.org/10.3390/atmos12030323

Ma Q, Zhang C, Liu C, He G, Zhang P, Li H, Chu B, He H (2023) A review on the heterogeneous oxidation of SO_2 on solid atmospheric particles: Implications for sulfate formation in haze chemistry. Crit Rev Env Sci Tec 53(21), 1888–1911. https://doi.org/10.1080/10643389.2023.2190315

Mahura A, Baklanov A, Makkonen R, Boy M, Petäjä T, Lappalainen HK, Nuterman R, Kerminen V-M, Arnold SR, Jochum M, Shvidenko A, Esau I, Sofiev M, Stohl A, Aalto T, Bai J, Chen C, Cheng Y, Drofa O, Huang M, Järvi L, Kokkola H, Kouznetsov R, Li T, Malguzzi P, Monks S, Poulsen MB, Noe SM, Palamarchuk Y, Foreback B, Clusius P, Rasmussen TAS, She J, Sørensen JH, Spracklen D, Su H, Tonttila J, Wang S, Wang J, Wolf-Grosse T, Yu Y, Zhang Q, Zhang W, Zhang W, Zheng X, Li S, Li Y, Zhou P, Kulmala M (2024) Towards seamless environmental prediction – development of Pan-Eurasian EXperiment (PEEX) modelling platform. Big Earth Data 8(2), 189-230. https://doi.org/10.1080/20964471.2024.2325019

Ministry of Ecology and Environment of the People's Republic of China (2016) Ambient air quality standards.

https://english.mee.gov.cn/Resources/standards/Air_Environment/quality_standard1/201605/t20160511_337502.shtml. Accessed 2 December 2024

Morawska L, Zhu T, Liu N, Torkmahalleh MA, Andrade MdF, Barratt B, Broomandi P, Buonanno G, Ceron LCB, Chen J, Cheng Y, Evans G, Gavidia M, Guo H, Hanigan I, Hu M, Jeong CH, Kelly F, Gallardo L, Kumar P, Lyu X, Mullins BJ, Nordstrøm C, Pereira G, Querol X, Roa NYR, Russell A, Thompson H, Wang H, Wang L, Wang T, Wierzbicka A, Xue T, Ye C (2021) The State of Science on Severe Air Pollution Episodes: Quantitative and Qualitative Analysis. Environ Int 156, 106732. https://doi.org/10.1016/j.envint.2021.106732

Nannoolal Y, Rarey J, Ramjugernath D (2008). Estimation of pure component properties: Part 3. Estimation of the vapor pressure of non-electrolyte organic compounds via group contributions and group interactions. Fluid Ph Equilib 269, 1-2:117-133. https://doi.org/10.1016/j.fluid.2008.04.020

National Centers for Environmental Prediction/National Weather Service/NOAA/US Department of Commerce (2000) NCEP FNL Operational Model Global Tropospheric Analyses, continuing from July 1999. Research Data Archive at the National Center for Atmospheric Research, Computational and Information Systems Laboratory. Dataset. https://doi.org/10.5065/D6M043C6

Ni Z, Luo K, Zhang J, Feng R, Zheng H, Zhu H, Wang J, Fan J, Gao X, Cen K (2018) Assessment of winter air pollution episodes using long-range transport modeling in Hangzhou, China, during World Internet Conference, 2015. Environ Pollut 236, 550-561. https://doi.org/10.1016/j.envpol.2018.01.069

Nightingale P, Malin G, Law C, Watson A, Liss P, Liddicoat M, Boutin J, Upstill-Goddard R (2000) In situ evaluation of air-sea gas exchange parameterizations using novel conservative and volatile tracers. Global Biogeochem Cy 14, 373-387. https://doi.org/10.1029/1999GB900091

Olenius T, Kupiainen-Määttä O, Ortega IK, Kurtén T, Vehkamäki H (2013) Free energy barrier in the growth of sulfuric acid–ammonia and sulfuric acid–dimethylamine clusters. J Chem Phys 139, 084312. https://doi.org/10.1063/1.4819024

Organisation for Economic Co-operation and Development (OECD) (2016) The economic consequences of outdoor air pollution. https://doi.org/10.1787/9789264257474-en

Paasonen P, Kupiainen K, Klimont Z, Visschedijk A, Denier van der Gon HAC, Amann M (2016) Continental anthropogenic primary particle number emissions. Atmos Chem Phys 16, 6823–6840. https://doi.org/10.5194/acp-16-6823-2016

Peltonen M (2017) University of Helsinki builds an air quality measuring station in Beijing, University of Helsinki. https://www.helsinki.fi/en/news/climate-change-and-biodiversity/university-helsinki-builds-air-quality-measuring-station-beijing. Accessed 1 November 2024

Pichelstorfer L, Roldin P, Rissanen M, Hyytinen N, Garmash O, Xavier C, Zhou P, Clusius P, Foreback B, Almeida TG, Deng C, Baykara M, Kurten T, Boy, M (2024) Towards automated inclusion of autoxidation chemistry in models: from precursors to atmospheric implications. Environmental Science: Atmospheres 4, 879-896. https://doi.org/10.1039/D4EA00054D

Pisso I, Sollum E, Grythe H, Kristiansen NI, Cassiani M, Eckhardt S, Arnold D, Morton D, Thompson RL, Zwaaftink CDG, Evangeliou N, Sodemann H, Haimberger L, Henne S, Brunner D, Burkhart JF, Fouilloux A, Brioude J, Philipp A, Seibert P, Stohl A (2019) The Lagrangian particle dispersion model FLEXPART version 10.4. Geosci Model Dev 12, 4955–4997. https://doi.org/10.5194/gmd-12-4955-2019

Reuters (2018) Northern China smog worsens in October-November as pace of restrictions eases: Greenpeace. https://www.reuters.com/article/idUSKBN1OC05S. Accessed 18 April 2024.

Roldin P, Swietlicki E, Schurgers G, Arneth A, Lehtinen KEJ, Boy M, Kulmala M (2011) Development and evaluation of the aerosol dynamics and gas phase chemistry model ADCHEM. Atmos Chem Phys 11, 5867–5896. https://doi.org/10.5194/acp-11-5867-2011

Roldin P, Ehn M, Kurtén T, Olenius T, Rissanen MP, Sarnela N, Elm J, Rantala P, Hao L, Hyttinen N, Heikkinen L, Worsnop DR, Pichelstorfer L, Xavier C, Clusius P, Öström E, Petäjä T, Kulmala M, Vehkamäki H, Virtanen A, Riipinen I, Boy M (2019) The role of highly oxygenated organic molecules in the Boreal aerosol-cloud-climate system. Nat Commun 10, 4370. https://doi.org/10.1038/s41467-019-12338-8

Rönkkö T, Kuuluvainen H, Karjalainen P, Keskinen J, Hillamo R, Niemi Jarkko V, Pirjola L, Timonen Hilkka J, Saarikoski S, Saukko E, Järvinen A, Silvennoinen H, Rostedt A, Olin M, Yli-Ojanperä J, Nousiainen P, Kousa A, Dal Maso M (2017) Traffic is a major source of atmospheric nanocluster aerosol. P Natl Acad Sci USA 114(29), 7549–7554. https://doi.org/10.1073/pnas.1700830114

Saide PE, Gao M, Lu Z, Goldberg DL, Streets DG, Woo J-H, Beyersdorf A, Corr CA, Thornhill KL, Anderson B, Hair JW, Nehrir AR, Diskin GS, Jimenez JL, Nault BA, Campuzano-Jost P, Dibb J, Heim E, Lamb KD, Schwarz JP, Perring AE, Kim J, Choi M, Holben B, Pfister G, Hodzic A, Carmichael GR, Emmons L, Crawford JH (2020) Understanding and improving model representation of aerosol optical properties for a Chinese haze event measured during KORUS-AQ. Atmos Chem Phys 20, 6455–6478. https://doi.org/10.5194/acp-20-6455-2020

Saunders SM, Jenkin ME, Derwent RG, Pilling MJ (2003) Protocol for the development of the Master Chemical Mechanism, MCM v3 (Part A): tropospheric degradation of non-aromatic volatile organic compounds. Atmos Chem Phys 3, 161–180. https://doi.org/10.5194/acp-3-161-2003

Seibert P, Frank A (2004) Source-receptor matrix calculation with a Lagrangian particle dispersion model in backward mode. Atmos Chem Phys 4, 51–63. https://doi.org/10.5194/acp-4-51-2004

Shen L, Wang H, Gao W, Yang Y, Huang W, Wang L, Zhang R, Zou J, Ji D, Wang Y (2020) Real-time physiochemistry of urban aerosols during a regional haze episode by a single-particle aerosol mass spectrometer: Mixing state, size distribution and source apportionment. Atmos Pollut Res 11(8), 1329-1338. https://doi.org/10.1016/j.apr.2020.05.010

Simpson D, Benedictow A, Darras S (2023) The CAMS soil emissions: CAMS-GLOB-SOIL, in: CAMS2_61 – Global and European emission inventories. Documentation of CAMS emission inventory products, 59–70. https://doi.org/10.24380/q2si-ti6i5

Sindelarova K, Granier C, Bouarar I, Guenther A, Tilmes S, Stavrakou T, Müller J-F, Kuhn U, Stefani P, Knorr W (2014) Global data set of biogenic VOC emissions calculated by the MEGAN model over the last 30 years. Atmos Chem Phys 14, 9317–9341. https://doi.org/10.5194/acp-14-9317-2014

Sindelarova K, Markova J, Simpson D, Huszar P, Karlicky J, Darras S, Granier C (2022) High-resolution biogenic global emission inventory for the time period 2000–2019 for air quality modelling. Earth Syst Sci Data 14, 251–270. https://doi.org/10.5194/essd-14-251-2022

Snyder EG, Watkins TH, Solomon PA, Thoma ED, Williams RW, Hagler GSW, Shelow D, Hindin DA, Kilaru VJ, Preuss PW (2013) The Changing Paradigm of Air Pollution Monitoring. Environ Sci Technol 47, 20, 11369–11377. https://doi.org/10.1021/es4022602

Sokhi RS, Moussiopoulos N, Baklanov A, Bartzis J, Coll I, Finardi S, Friedrich R, Geels C, Grönholm T, Halenka T, Ketzel M, Maragkidou A, Matthias V, Moldanova J, Ntziachristos L, Schäfer K, Suppan P, Tsegas G, Carmichael G, Franco V, Hanna S, Jalkanen J-P, Velders GJM, Kukkonen J (2022) Advances in air quality research – current and emerging challenges. Atmos Chem Phys 22, 4615–4703. https://doi.org/10.5194/acp-22-4615-2022

Song C, Wu L, Xie Y, He J, Chen X, Wang T, Lin Y, Jin T, Wang A, Liu Y, Dai Q, Liu B, Wang Y, Mao H (2017) Air pollution in China: Status and spatiotemporal variations. Environ Pollut 227, 334-347. https://doi.org/10.1016/j.envpol.2017.04.075

Soulie A, Granier C, Darras S, Zilbermann N, Doumbia T, Guevara M, Jalkanen J-P, Keita S, Liousse C, Crippa M, Guizzardi D, Hoesly R, Smith SJ (2024) Global anthropogenic emissions (CAMS-GLOB-ANT) for the Copernicus Atmosphere Monitoring Service simulations of air quality forecasts and reanalyses. Earth Syst Sci Data 16, 2261–2279. https://doi.org/10.5194/essd-16-2261-2024

Stohl A, Hittenberger M, Wotawa G (1998) Validation of the Lagrangian particle dispersion model FLEXPART against large scale tracer experiments. Atmos Environ 32, 4245-4264. https://doi.org/10.1016/S1352-2310(98)00184-8

Stohl A, Thomson DJ (1999) A density correction for Lagrangian particle dispersion models. Bound-Layer Met 90, 155-167. https://doi.org/10.1023/A:1001741110696

Stohl A, Forster C, Frank A, Seibert P, Wotawa G (2005) Technical note: The Lagrangian particle dispersion model FLEXPART version 6.2. Atmos Chem Phys 5, 2461–2474. https://doi.org/10.5194/acp-5-2461-2005

Sun C, Zheng S, Wang R (2014). Restricting driving for better traffic and clearer skies: Did it work in Beijing? Transport Policy 32, 34-41. https://doi.org/10.1016/j.tranpol.2013.12.010

Su H, Cheng Y, Pöschl U (2020) New Multiphase Chemical Processes Influencing Atmospheric Aerosols, Air Quality, and Climate in the Anthropocene. Acc Chem Res 53, 10, 2034–2043. https://doi.org/10.1021/acs.accounts.0c00246

Sun J, Huang L, Liao H, Li J, Hu J (2017) Impacts of Regional Transport on Particulate Matter Pollution in China: a Review of Methods and Results. Curr Pollut Rep 3, 182–191. https://doi.org/10.1007/s40726-017-0065-5

Sun L, Zhang T, Liu S, Wang K, Rogers T, Yao L, Zhao P (2021) Reducing energy consumption and pollution in the urban transportation sector: A review of policies and regulations in Beijing. J Clean Prod 285, 125339. https://doi.org/10.1016/j.jclepro.2020.125339

Sun W, Shao M, Granier C, Liu Y, Ye CS, Zheng JY (2018) Long-Term Trends of Anthropogenic SO_2, NO_x, CO, and NMVOCs Emissions in China. Earth's Future 6 (8), 1112–1133. https://doi.org/10.1029/2018ef000822

Sun YL, Wang ZF, Du W, Zhang Q, Wang QQ, Fu P Q, Pan XL, Li J, Jayne J, Worsnop DR (2015) Long-term real-time measurements of aerosol particle composition in Beijing, China: seasonal variations, meteorological effects, and source analysis. Atmos Chem Phys 15, 10149–10165. https://doi.org/10.5194/acp-15-10149-2015

Sun Y, Du W, Fu P, Wang Q, Li J, Ge X, Zhang Q, Zhu C, Ren L, Xu W, Zhao J, Han T, Worsnop DR, Wang Z (2016) Primary and secondary aerosols in Beijing in winter: sources, variations and processes. Atmos Chem Phys 16, 8309–8329. https://doi.org/10.5194/acp-16-8309-2016

Tao M, Chen L, Li R, Wang L, Wang J, Wang Z, Tang G, Tao J (2016) Spatial Oscillation of the particle pollution in eastern China during winter: Implications for regional air quality and climate. Atmos Environ 144, 100-110. https://doi.org/10.1016/j.atmosenv.2016.08.049

Thunis P, Miranda A, Baldasano JM, Blond N, Douros J, Graff A, Janssen S, Juda-Rezler K, Karvosenoja N, Maffeis G, Martilli A, Rasoloharimahefa M, Real E, Viaene P, Volta M, White L (2016) Overview of current regional and local scale air quality modelling practices: Assessment and planning tools in the EU. Environ Sci Policy 65, 13-21. https://doi.org/10.1016/j.envsci.2016.03.013

Tipka A, Haimberger L, Seibert P (2020) Flex_extract v7.12 – a software package to retrieve and prepare ECMWF data for use in FLEXPART. Geosci Model Dev 13, 5277–5310. https://doi.org/10.5194/gmd-13-5277-2020

Tiwari V, Hanai Y, Masunaga S (2010) Ambient levels of volatile organic compounds in the vicinity of petrochemical industrial area of Yokohama, Japan. Air Qual Atmos Hlth 3, 65–75. https://doi.org/10.1007/s11869-009-0052-0

Tong D, Geng G, Jiang K, Cheng J, Zheng Y, Hong C, Yan L, Zhang Y, Chen X, Bo Y, Lei Y, Zhang Q, He K (2019) Energy and emission pathways towards $PM_{2.5}$ air quality attainment in the Beijing-Tianjin-Hebei region by 2030. Sci Total Environ 692, 361-370. https://doi.org/10.1016/j.scitotenv.2019.07.218

US EPA (2007) Guidance on the Use of Models and Other Analyses for Demonstrating Attainment of Air Quality Goals for Ozone, $PM_{2.5}$, and Regional Haze, Vol EPA-454/B-07e002, U. S. Environmental Protection Agency, Research Triangle Park, NC.

van den Elshout S, Léger K, Nussio F (2008) Comparing urban air quality in Europe in real time: A review of existing air quality indices and the proposal of a common alternative. Environ Int 34, 720-726. https://doi.org/10.1016/j.envint.2007.12.011

Wang K, Ma X, Tian R, Yu F (2023) Analysis of new particle formation events and comparisons to simulations of particle number concentrations based on GEOS-Chem–advanced particle microphysics in Beijing, China. Atmos Chem Phys 23, 4091–4104. https://doi.org/10.5194/acp-23-4091-2023

Wang L, Liu Z, Sun Y, Ji D, Wang Y (2015) Long-range transport and regional sources of $PM_{2.5}$ in Beijing based on long-term observations from 2005 to 2010. Atmos Res 157, 37-48. https://doi.org/10.1016/j.atmosres.2014.12.003

Wang S, Hao J (2012) Air quality management in China: Issues, challenges, and options. J Environ Sci 24:1, 2-13. https://doi.org/10.1016/S1001-0742(11)60724-9

Wang T, Liu H, Li J, Wang S, Kim Y, Sun Y, Yang W, Du H, Wang Z, Wang Z (2023b). A two-way coupled regional urban–street network air quality model system for Beijing, China. Geosci Model Dev 16, 5585–5599. https://doi.org/10.5194/gmd-16-5585-2023

Wang Y, Bao S, Wang S, Hu Y, Shi X, Wang J, Zhao B, Jiang J, Zheng M, Wu M, Russell AG, Wang Y, Hao J (2017) Local and regional contributions to fine particulate matter in Beijing during heavy haze episodes. Sci Total Environ 580, 283–296. https://doi.org/10.1016/j.scitotenv.2016.12.127

Wang Y, Dörner S, Donner S, Böhnke S, De Smedt I, Dickerson RR, Dong Z, He H, Li Z, Li Z, Li D, Liu D, Ren X, Theys N, Wang Y, Wang Y, Wang Z, Xu H, Xu J, Wagner T (2019) Vertical profiles of NO2, SO2, HONO, HCHO, CHOCHO and aerosols derived from MAX-DOAS measurements at a rural site in the central western North China Plain and their relation to emission sources and effects of regional transport. Atmos Chem Phys 19, 5417–5449. https://doi.org/10.5194/acp-19-5417-2019

Wang Y, Yu M, Wang Y, Tang G, Song T, Zhou P, Liu Z, Hu B, Ji D, Wang L, Zhu X, Yan C, Ehn M, Gao W, Pan Y, Xin J, Sun Y, Kerminen V-M, Kulmala M, Petäjä T (2020) Rapid formation of intense haze episodes via aerosol–boundary layer feedback in Beijing. Atmos Chem Phys 20, 45–53. https://doi.org/10.5194/acp-20-45-2020

Weather Underground (2024) Beijing, People's Republic of China Weather History, Beijing Capital International Airport Station. https://www.wunderground.com/history/daily/cn/beijing/ZBAA/. Accessed 29 April 2024

Westervelt DM, Horowitz LW, Naik V, Tai APK, Fiore AM, Mauzerall DL (2016) Quantifying $PM_{2.5}$-meteorology sensitivities in a global climate model. Atmos Environ 142, 43-56. https://doi.org/10.1016/j.atmosenv.2016.07.040

WHO (World Health Organization) (2021) WHO global air quality guidelines: Particulate matter ($PM_{2.5}$ and PM_{10}), ozone, nitrogen dioxide, sulfur dioxide and carbon monoxide. World Health Organization, Geneva. https://iris.who.int/handle/10665/345329. License: CC BY-NC-SA 3.0 IGO

WHO (World Health Organization) (2024). Air quality, energy and health: Health impacts. https://www.who.int/teams/environment-climate-change-and-health/air-quality-energy-and-health/health-impacts. Accessed 1 November 2024

Wieder WR, Boehnert J, Bonan GB, Langseth M (2014) Regridded Harmonized World Soil Database v1.2 ORNL DAAC, Oak Ridge, Tennessee, USA. https://doi.org/10.3334/ORNLDAAC/1247

Williams RS, Hegglin MI, Kerridge BJ, Jöckel P, Latter BG, Plummer DA (2019) Characterising the seasonal and geographical variability in tropospheric ozone, stratospheric influence and recent changes. Atmos Chem Phys 19, 3589–3620. https://doi.org/10.5194/acp-19-3589-2019

Wu J, Bei N, Wang Y, Li X, Liu S, Liu L, Wang R, Yu J, Le T, Zuo M, Shen Z, Cao J, Tie X, Li G (2021) Insights into particulate matter pollution in the North China Plain during wintertime: local contribution or regional transport? Atmos Chem Phys 21, 2229–2249. https://doi.org/10.5194/acp-21-2229-2021

Xausa F, Paasonen P, Makkonen R, Arshinov M, Ding A, Denier Van Der Gon H, Kerminen V-M Kulmala M (2018) Advancing global aerosol simulations with size-segregated anthropogenic particle number emissions. Atmos Chem Phys 18, 10039–10054. https://doi.org/10.5194/acp-18-10039-2018

Xiao C, Chang M, Guo P, Gu M, Li Y (2020) Analysis of air quality characteristics of Beijing–Tianjin–Hebei and its surrounding air pollution transport channel cities in China. J Environ Sci 87, 213-227. https://doi.org/10.1016/j.jes.2019.05.024

Xie Y, Dai H, Zhang Y, Wu Y, Hanaoka T, Masui T (2019) Comparison of health and economic impacts of $PM_{2.5}$ and ozone pollution in China. Environ Int 130, 104881. https://doi.org/10.1016/j.envint.2019.05.075

Xu L, Fan X, Wang W, Xu L, Duan Y, Shi R (2017) Renewable and sustainable energy of Xinjiang and development strategy of node areas in the “Silk Road Economic Belt”. Renew Sust Energ Rev 79, 274-285. https://doi.org/10.1016/j.rser.2017.05.031

Xue Y, Zhou Z, Nie T, Wang K, Nie L, Pan T, Wu X, Tian H, Zhong L, Li J, Liu H, Liu S, Shao P (2016) Trends of multiple air pollutants emissions from residential coal combustion in Beijing and its implication on improving air quality for control measures. Atmos Environ 142, 303-3012. https://doi.org/10.1016/j.atmosenv.2016.08.004

Yan Y, Zhou Y, Kong S, Lin J, Wu J, Zheng H, Zhang Z, Song A, Bai Y, Ling Z, Liu D, Zhao T (2021) Effectiveness of emission control in reducing $PM_{2.5}$ pollution in central China during winter haze episodes under various potential synoptic controls. Atmos Chem Phys 21, 3143–3162. https://doi.org/10.5194/acp-21-3143-2021

Yang J, Ji Z, Kang S, Zhang Q, Chen X, Lee S-Y (2019) Spatiotemporal variations of air pollutants in western China and their relationship to meteorological factors and emission sources. Environ Pollut 254, 112952. https://doi.org/10.1016/j.envpol.2019.07.120

Yang W, Wang G, Bi C (2017) Analysis of Long-Range Transport Effects on $PM_{2.5}$ during a Short Severe Haze in Beijing, China. Aerosol Air Qual Res 17, 1610-1622. https://doi.org/10.4209/aaqr.2016.06.0220

Yang Y, Liao H, Lou S (2016). Increase in winter haze over eastern China in recent decades: Roles of variations in meteorological parameters and anthropogenic emissions. J Geophys Res-Atmos 121, 13050–13065. https://doi.org/10.1002/2016jd025136

Zeng Y, Cao Y, Qiao X, Seyler BC, Tang Y (2019) Air pollution reduction in China: Recent success but great challenge for the future. Sci Total Environ 663, 329-337. https://doi.org/10.1016/j.scitotenv.2019.01.262

Zhai H, Huang L, Emery C, Zhang X, Wang Y, Yarwood G, Fu JS, Li L (2024) Recommendations on benchmarks for photochemical air quality model applications in China — NO_2, SO_2, CO and PM_{10}. Atmos Environ 319, 120290. https://doi.org/10.1016/j.atmosenv.2023.120290

Zhang H, Cheng S, Li J, Yao S, Wang X (2019) Investigating the aerosol mass and chemical components characteristics and feedback effects on the meteorological factors in the Beijing-Tianjin-Hebei region, China. Environ Pollut 244, 495-502. https://doi.org/10.1016/j.envpol.2018.10.087

Zhang J, Liu L, Xu L, Lin Q, Zhao H, Wang Z, Guo S, Hu M, Liu D, Shi Z, Huang D, Li W (2020a) Exploring wintertime regional haze in northeast China: role of coal and biomass burning. Atmos Chem Phys 20, 5355–5372. https://doi.org/10.5194/acp-20-5355-2020

Zhang R, Chen C, Liu S, Wu H, Zhou W, Li P (2024a). Impact of "coal to electricity" policy on air quality during heating period over Beijing − Tianjin − Hebei region in China by WRF-Chem model. Air Qual Atmos Hlth. https://doi.org/10.1007/s11869-024-01685-1

Zhang T, de Jong MC, Wooster MJ, Xu W, Wang L (2020b) Trends in eastern China agricultural fire emissions derived from a combination of geostationary (Himawari) and polar (VIIRS) orbiter fire radiative power products. Atmos Chem Phys 20, 10687–10705. https://doi.org/10.5194/acp-20-10687-2020

Zhang T, Gu Y, Zhao B, Wang L, Zhu Z, Lin Y, Chang X, Xia X, Jiang Z, Shi H, Gong W (2024b). Observation-based quantification of aerosol transport using optical flow: A satellite perspective to characterize interregional transport of atmospheric pollution. Remote Sens Environ 315, 114457. https://doi.org/10.1016/j.rse.2024.114457

Zhang X, Zhong J, Wang J, Wang Y, Liu Y (2018) The interdecadal worsening of weather conditions affecting aerosol pollution in the Beijing area in relation to climate warming. Atmos Chem Phys 18, 5991–5999. https://doi.org/10.5194/acp-18-5991-2018

Zhang Y, Zhang X, Wang L, Zhang Q, Duan F, He K (2016) Application of WRF/Chem over East Asia: Part I. Model evaluation and intercomparison with MM5/CMAQ. Atmos Environ 124B, 285-300. https://doi.org/10.1016/j.atmosenv.2015.07.022

Zhang Z, Wang X, Zhang Y, Lü S, Huang Z, Huang X, Wang Y (2015) Ambient air benzene at background sites in China's most developed coastal regions: Exposure levels, source implications and health risks. Sci Total Environ 511, 792-800. https://doi.org/10.1016/j.scitotenv.2015.01.003

Zhang Z, Wang W, Cheng M, Liu S, Xu J, He Y, Meng F (2017) The contribution of residential coal combustion to $PM_{2.5}$ pollution over China's Beijing-Tianjin-Hebei region in winter. Atmos Environ, 159, 147-161. https://doi.org/10.1016/j.atmosenv.2017.03.054

Zhao G, Guerrero JM, Jiang K, Chen, S (2017) Energy modelling towards low carbon development of Beijing in 2030. Energy 121, 107-113. http://dx.doi.org/10.1016/j.energy.2017.01.019

Zhao D, Xin J, Gong C, Quan J, Liu G, Zhao W, Liu Z, Song T (2019) The formation mechanism of air pollution episodes in Beijing city: Insights into the measured feedback between aerosol radiative forcing and the atmospheric boundary layer stability. Sci Total Environ 692, 371-381. https://doi.org/10.1016/j.scitotenv.2019.07.255

Zheng GJ, Duan FK, Su H, Ma YL, Cheng Y, Zheng B, Zhang Q, Huang T, Kimoto T, Chang D, Pöschl U, Cheng YF, He KB (2015a) Exploring the severe winter haze in Beijing: the impact of synoptic weather, regional transport and heterogeneous reactions. Atmos Chem Phys 15, 2969–2983. https://doi.org/10.5194/acp-15-2969-2015

Zheng G, Duan F, Ma Y, Zhang Q, Huang T, Kimoto T, Cheng Y, Su H, He K (2016) Episode-Based Evolution Pattern Analysis of Haze Pollution: Method Development and Results from Beijing, China. Environ Sci Technol 50, 4632-4641. https://doi.org/10.1021/acs.est.5b05593

Zheng XY, Fu YF, Yang YJ, Liu GS (2015b) Impact of atmospheric circulations on aerosol distributions in autumn over eastern China: observational evidence. Atmos Chem Phys 15, 12115–12138. https://doi.org/10.5194/acp-15-12115-2015

Zhou L, Nieminen T, Mogensen D, Smolander S, Rusanen A, Kulmala M, Boy M (2014) SOSAA — a new model to simulate the concentrations of organic vapours, sulphuric acid and aerosols inside the ABL — Part 2: Aerosol dynamics and one case study at a boreal forest site. Boreal Environ Res 19 (suppl. B), 237–256

Ziska F, Quack B, Abrahamsson K, Archer SD, Atlas E, Bell T, Butler JH, Carpenter LJ, Jones CE, Harris NRP, Hepach H, Heumann KG, Hughes C, Kuss J, Krüger K, Liss P, Moore RM, Orlikowska A, Raimund S, Reeves CE, Reifenhäuser W, Robinson AD, Schall C, Tanhua T, Tegtmeier S, Turner S, Wang L, Wallace D, Williams J, Yamamoto H, Yvon-Lewis S, Yokouchi Y (2013) Global sea-to-air flux climatology for bromoform, dibromomethane and methyl iodide. Atmos Chem Phys 13, 8915–8934. https://doi.org/10.5194/acp-13-8915-2013